FLIGHT ENVIRONMENT OF THE PROPELLERS ON COMMUTER AIRCRAFT

A Thesis by

Johann Dorfling

BS Mechanical Engineering, University of Kentucky, 2007

Submitted to the Department of Aerospace Engineering
and the faculty of the Graduate School of
Wichita State University
in partial fulfillment of
the requirements for the degree
Master of Science

December 2008

FLIGHT ENVIRONMENT OF THE PROPELLERS ON COMMUTER AIRCRAFT

The following faculty members have examined the final copy of this thesis for form and content, and recommend that it be accepted in partial fulfillment of the requirements for the degree of Master of Science with a major in Aerospace Engineering.

_____

Kamran Rokhsaz, Committee Chair

_____

James Steck, Committee Member

_____

Hamid Lankarani, Committee Member

DEDICATION

This thesis is dedicated to my parents. Thank you
for your ceaseless love and support.

ABSTRACT

Data obtained from digital flight data recorders installed on a fleet of 27 Beech 1900Ds are used to assess the actual operational environment of propellers on commuter aircraft. The data consists of 910 complete flights and 589 flight hours. Aircraft operations have been separated into three ground operations categories and five flight phases. Parameters that pertain to the propellers are emphasized. Overall aircraft and subsystem usage is also considered to establish the commuter airline flight profile.

Overall aircraft usage includes information on flight durations and time within each flight phase, time at various airspeeds and engine torque levels, and flap operations. Flights of commuter aircraft are shown to be of short duration, with the cruise phase accounting for the majority of airborne time.

Ground phases highlight the operation of the propellers within prohibited shaft speed ranges. A noticeable length of time is shown to have been spent within these restricted ranges. The usage of reverse thrust during landing rollouts and ground operations is also considered. Reversals upon landing accounted for less than half of the total number of reverse cycles.

The short duration takeoff rotation is shown to impose the most severe operating conditions on the propellers. Aerodynamic parameters indicate large inflow angles into the propeller disk, resulting in the most severe vibratory loads. Engine torque, propeller shaft speed, and airspeed are all considered as contributing factors to the large vibratory loads the propellers experience at takeoff rotation.

Information pertaining to the in flight engine and propeller usage is also given, and shows no abnormal usage of these components. Cumulative frequency of occurrence of angle of attack for each of the five flight phases has been normalized per 1000 hours and per nautical mile. Each

flight phase is shown to produce a unique pattern of frequency of occurrence of the angle of attack, driven by the associated airspeeds. Another aerodynamic parameter considered while in flight is the upwash angle. Upwash angle has been derived for a variety of aircraft weights and airspeeds. This parameter is shown to have a significant influence on the propeller inflow angle, especially at high aircraft weight and low airspeed conditions.

The change in inflow angle due to gusts has also been extracted and normalized per 1000 hours and per nautical mile. This data is given in the form of plots of cumulative frequency of occurrence for each flight phase and altitude. Increasing altitude shows a significant reduction in the frequency and magnitude of variations in angle of attack caused by gusts.

The information is presented in statistical formats that could enable the FAA, the propeller manufacturer, and the airline to better understand and control those factors that influence the structural integrity of these components.

TABLE OF CONTENTS

TABLE OF CONTENTS (Continued)

LIST OF TABLES

LIST OF FIGURES

LIST OF FIGURES (Continued)

NOMENCLATURE

a	local speed of sound, ft/s
a_{ISA}	ISA sea level speed of sound, ft/s
A_r	wing aspect ratio, b^2/S
b	wingspan, ft
b_e	equivalent wingspan, $\pi b/4$
$\bar{c}$	wing mean geometric chord, ft
$\overline{C}$	aircraft derived gust response factor
$C_{L\alpha}$	airplane lift curve slope per radian
C_P	power coefficient
C_T	thrust coefficient
D	propeller diameter, ft
g	gravitational constant, 32.17 ft/s²
h	perpendicular distance from vortex to point of interest, ft
H	altitude, ft
H_P	pressure altitude, ft
J	advance ratio, V_T/nD
K_g	derived gust alleviation factor, $0.88\mu_g/(5.3+\mu_g)$
L	lift, lbf
M_∞	free stream Mach number, V_T/a
M_{tip}	propeller tip Mach number

NOMENCLATURE (Continued)

n	propeller shaft speed, RPS
n_z	vertical load factor, g
P	power, ft-lbf/s
Q	torque, ft-lbf
r	distance from vortex element to point of interest, ft
r_B	blade element radial position, ft
s	distance from vortex element to point on vortex normal to point of interest, ft
S	wing area, ft²
T	thrust, lbf
U_{de}	derived gust velocity, ft/s
v	vortex induced velocity, ft/s
V_e	equivalent airspeed, ft/s
V_R	propeller blade relative velocity, ft/s
V_T	true airspeed, ft/s
V_v	vertical speed, ft/s
W	weight, lbf

Greek Symbols

α	angle of attack
α_B	propeller blade angle of attack
β	Mach number correction, $\sqrt{1-M_\infty^2}$

NOMENCLATURE (Continued)

β_B	propeller blade pitch angle
γ	flight path angle
Γ	vortex strength, ft²/s
η	angle used in calculation of velocity induced by a vortex filament
θ	aircraft pitch angle
λ	angle used in calculation of velocity induced by a vortex filament
μ	mean of a population
μ_g	aircraft mass parameter (non-dimensional)
ν	angle used in calculation of velocity induced by a vortex filament
ρ_∞	local air density, slugs/ft³
ρ_{ISA}	ISA sea level air density, 0.0023769 slugs/ft³
σ	standard deviation of a population
φ	effective propeller blade pitch angle
ϕ	angle used in calculation of velocity induced by a vortex filament
ψ	inflow angle

Acronyms

DFDR	Digital Flight Data Recorder
DOS	Disk Operating System
FAA	Federal Aviation Administration
FPM	Feet Per Minute

NOMENCLATURE (Continued)

IAS	Indicated Airspeed
ICAO	International Civil Aviation Organization
ISA	ICAO Standard Atmosphere
KIAS	Knots, Indicated Airspeed
KTAS	Knots, True Airspeed
RPM	Revolutions Per Minute
RPS	Revolutions Per Second
TAS	True Airspeed

I. INTRODUCTION

A. HISTORICAL CONTEXT

Propellers have been around since the dawn of aviation more than 100 years ago. The Wright brothers were the first to build and use an effective aerial propeller – a component without which their historical flight at Kitty Hawk on December 17, 1903 would never have taken place [1]. The propeller the Wrights used on their aircraft in 1903 was so revolutionary that this method of aircraft propulsion is still in widespread use on all types of aircraft today.

After the first powered flights, the science and understanding of propellers grew rapidly. Throughout World War II, sophisticated prop driven aircraft were used extensively for all types of missions. As the war drew to a close in 1945, the Germans ushered in the jet age with the Messerschmitt Me-262, and the Americans were not far behind with the Lockheed P-80. Jet aircraft offered one major advantage over their prop driven counterparts: speed.

The 1950s saw the introduction of many jet powered airliners. These airplanes offered quiet comfort and high cruise speeds – something with which piston and turboprop aircraft of the time could not compete. It must have been during this time period that the public began perceiving propeller driven aircraft as outdated. But propellers never disappeared and were still widely used on personal, freight, military, and even on some passenger aircraft.

During the energy crisis of the 1970s and 80s, airlines suffered severely under the high fuel prices. As a result, NASA launched a program that researched methods of improving aircraft fuel efficiency. The Advanced Turboprop Project was the most revolutionary project that resulted from this program and held the greatest promise of increased fuel efficiency. This project explored propeller technology that would allow a turboprop to fly at cruise speeds of up

to Mach number of 0.8, similar to that of turbofan propelled commercial airliners. The result of this project was a turboprop derivative known as propfans. These propfans demonstrated that a propeller driven aircraft is capable of cruising at the same speeds as the turbofans while retaining the turboprop fuel efficiency advantage. The success of the project was marked in 1987 when the prestigious Collier Trophy was awarded to NASA's Lewis Research Center and the industry team that helped with the project [2]. The propfans that came out of this project could have made a major impact on the aviation industry, but unfortunately a sharp drop in oil prices made the new propfan technology too expensive and not economically viable to pursue further.

Now, 20 years later, airlines around the world are again faced with the same problem of high fuel prices. Turboprops are from 10% to 30% more fuel efficient than turbofan aircraft – thus the recent decrease in sales of regional jets in the 20-70 seat range, coupled with the sharp increase in turboprop sales, is hardly surprising [3, 4]. The two major players in the turboprop airline market – Bombardier and ATR – both reported record turboprop sales in 2007. Bombardier reported a total of 80 orders for their Q400 turboprop aircraft, while in 2006 this aircraft only received 24 orders. At the same time, they only received 70 orders for the CRJ900 regional jet, a 40% decrease from 2006 [5]. Finmeccanica, a parent company of ATR, reported 123 orders in 2007 for the ATR 42-500 and ATR 72-500 turboprops [6]. In 2006 a significantly smaller number of orders – 63 – were booked for these aircraft, though it was still more than the 2005 sales [7].

Turboprops are not capable of the same cruising speeds of jets yet, but in the commuter airline role with flights that are typically less than 500nm the speed difference is a moot point. Thus it makes more economical sense for airlines to fly turboprops on these shorter flights. The major obstacle facing the turboprop today is the public perception of propeller driven aircraft as

noisy, uncomfortable, and outdated. Such views will only change with time as more passengers fly on modern turboprop aircraft and realize that these aircraft are actually quieter and more spacious than the equivalent regional jets.

With the high oil prices, turboprops are fast becoming the preferred choice of aircraft in the commuter airline role. There will surely be more turboprop aircraft flying in the future, thus it is important to study the operational environment of propeller driven aircraft in the commuter role to aid in the improvement of safety as well as future regulations. It is also important to provide aircraft and propeller manufacturers with data that describe the usage of commuter aircraft and their components for the purpose of comparison and improvement of design assumptions. A review of literature indicated that there is little information in the open literature describing the actual operational environment of propellers on commuter aircraft. A study conducted by the University of Dayton Research Institute (UDRI) on the operational loads of a commuter aircraft are presented in reference 8. This study, however, focuses on the aircraft operational environment and loads, and not on the propeller usage.

B. COMPOSITE PROPELLERS

The Wright brothers' propeller that propelled the Wright Flyer was made from a composite material – wood. But as aircraft technology developed, aluminum propeller blades quickly became common, and wood composite propellers were almost completely phased out. In the past thirty years, there has been a widespread resurgence in the use of composite propeller blades; but now these propellers are constructed from carbon composite materials rather than wood. Carbon composite propeller blades provide a number of advantages over aluminum blades. The most important benefit of a carbon composite blade is perhaps a large decrease in

weight. With increasing diameter, the weight of aluminum propeller blades increases dramatically. This increased weight causes much higher centrifugal loads on the propeller hub assembly, and therefore limits the diameter and the number of blades that a hub assembly can accommodate.

Composites give designers the advantage of changing the layup of the material so that a propeller blade would not have any resonance frequencies within the operating range of the propeller – and this can be done without adversely affecting the strength or weight of the blade [9]. With aluminum blades, if a natural frequency is excited within the running range of the propeller, there is not much that can be done to the blade itself to alter its resonance frequency. This can often result in restricted propeller operating ranges [10].

When composite propellers were first being designed and produced, there was some skepticism about the composite materials' ability to withstand environmental factors such as solar radiation, moisture and lightning strikes. Studies conducted by Dowty Rotol Ltd and Hartzell Propeller Inc have shown that there has been no significant adverse effects on the mechanical properties of the blades which have been in service for up to ten years. Moisture content in a Dowty Rotol rotor blade that was in service for ten years was less than 0.4%, and there was no evidence of a reduction in the strength of the carbon fiber composite. Both companies conducted lightning strike tests on blade specimens, and neither noted any major damage to the blade nor any significant reduction in the strength of the blade [11, 12].

C. AIRCRAFT AND PROPELLER INFORMATION

1. Beech 1900D Airliner

The aircraft whose operation is under investigation in this study is the Beech 1900D airliner. The Beech 1900 airliner, derived from the Beechcraft King Air 200, made its maiden flight in 1982, and received its FAA certification in 1983. Since introducing the 19 seat airliner into service in 1984, Beechcraft has produced a number of variations of the 1900. After the production of three prototypes, the 1900C was introduced, of which 74 were produced. Shortly thereafter, the 1900C-1 was introduced and featured a wet-wing that allowed for higher fuel capacities. A total of 174 1900C-1s were produced up until 1991, when the 1900D was introduced. The 1900D model, shown in Figure 1, was given a number of improvements over the previous models. One of the major improvements was a larger cabin that allowed occupants to stand upright. As a result of the 28.5 percent increase in cabin size and the resulting increased weight, the aircraft was fitted with more powerful 1279 shaft horsepower Pratt & Whitney Canada PT6A-67D engines, each running a Hartzell Propeller Inc composite propeller. This was the first variant to employ composite propellers. Other modifications included the addition of winglets, which improved the aircraft's high density altitude performance, and a larger vertical stabilizer [13].

The 1900D was the most popular version of the airliner produced, with a total of 438 built during its production, which ran from 1991 to 2002. The majority of these airplanes found service in the commuter airline role. Table 1 presents some of the characteristics of the BE-1900D, and Table 2 the placarded speeds for the aircraft.

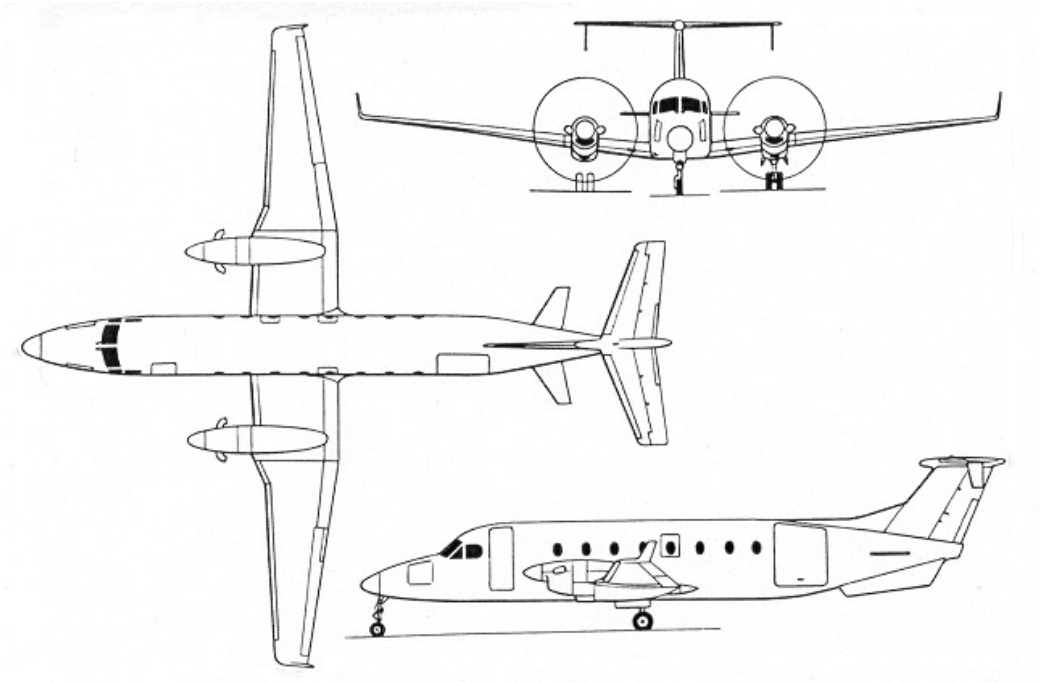

Figure 1. BE-1900D three-view schematic [13]

Table 1. BE-1900D aircraft characteristics [13]

Parameter	**Value**
Maximum Taxi Weight	17,060 lb
Maximum Takeoff Weight	16,950 lb
Maximum Landing Weight	16,600 lb
Zero-Fuel Weight	15,000 lb
Operating Empty Weight	10,350 lb
Fuel Capacity	668 U.S. gallons
Two P&W PT6A-67D	1,279 shp each
Wing Span	57 ft 11.25 in
Wing Reference Area	310 ft^2
Wing MAC	5.32 ft
Length	57 ft 10 in
Height	15 ft 6 in
Tread	17 ft 2 in
Wheel Base	23 ft 9.5 in

Table 2. BE-1900D placarded airspeeds

Speed	**KIAS**
Maximum Operating Speed (V_{MO})	
- Below 13,200 ft	248
- 13,200 to 25,000 ft	248-195 (0.48 Mach)
Maximum Flap Extension Airspeed (V_{FE})	
- Approach Flaps	188
- Full Flaps	154
Maximum Landing Gear Operating/Extended Airspeed (V_{LO}/V_{LE})	180
Stalling Speeds	
- Landing Gear and Flaps Up	101
- Landing Gear Down, Approach Flaps	90
- Landing Gear Down, Full Flaps	84
Minimum Control Airspeed (V_{MCA})	
- Flaps Up or Approach	92

2. Hartzell E10950 Composite Propeller Blades

The aircraft is fitted with two four bladed Hartzell Propeller Inc aramid composite, 110 inch diameter propellers [14]. The propeller construction consists of a polyurethene foam core covered with a laminated Kevlar* shell; two uni-directional Kevlar spars run along the leading and trailing edges of the blade. The blade attaches to an aluminum shank at its root which inserts into an aluminum hub assembly. The leading edge of the blade is covered with a metal strip for erosion prevention [11, 15]. Cross-sections of a composite propeller blade at the mid point and tip of the blade are shown in Figure 2.

* Kevlar is a registered trademark of E.I. du Pont de Nemours and Company

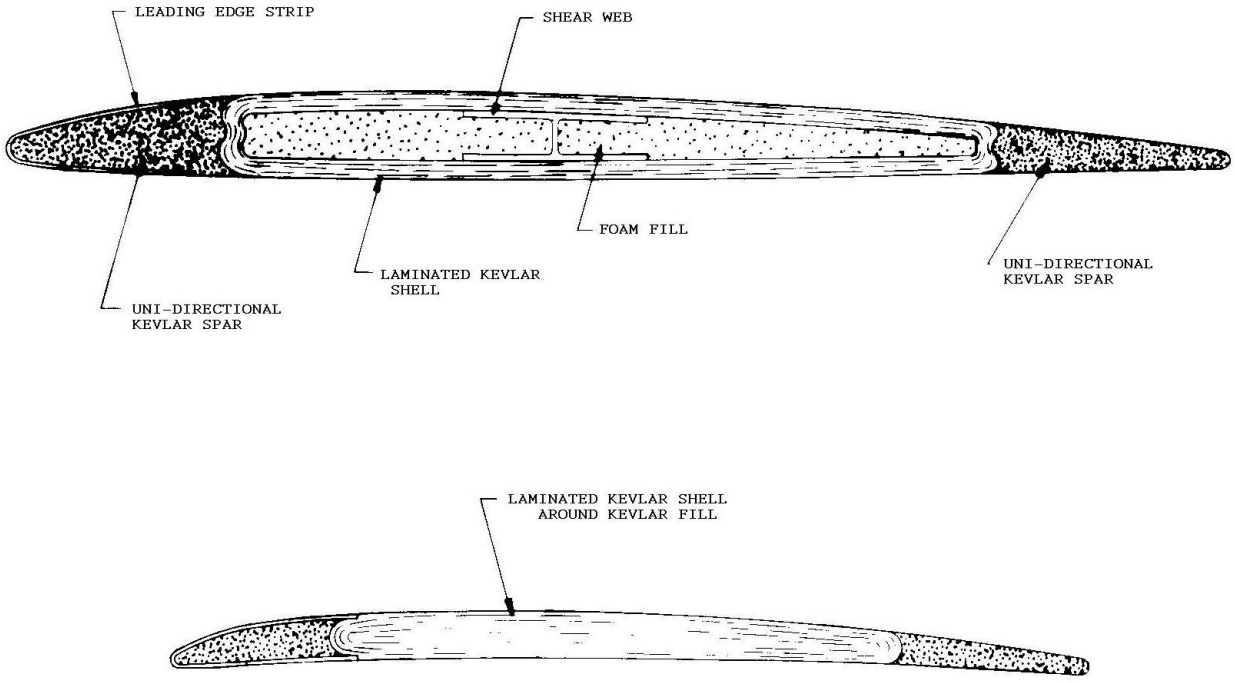

Figure 2. Mid-blade and blade tip cross-sections of a composite propeller blade showing the details of construction [15][†]

D. RESEARCH OBJECTIVE

Wichita State University is in possession of flight data from a fleet of Beech 1900D aircraft. This database consists of digital flight recorder data collected from 910 flights representing approximately 589 flight hours recorded on 27 aircraft during typical operational usage by a single commuter airline. The objective of this study is to define and describe the operational environment of the composite propellers on the 1900D. The ultimate goal is to provide the propeller manufacturers, the FAA, and the airline operator with actual propeller operational data to better understand and control those factors that influence the structural integrity of these components.

[†] Reprinted with permission from SAE Paper # 790579 © 1979 SAE International

E. ROADMAP TO THE FOLLOWING CHAPTERS

The method of analysis is discussed in Chapter II. The criteria used for the separation of the phases, as well as detailed discussions of the methods used to extract those parameters from the flight data files, are also presented. Particular attention is given to the propeller inflow angle and its effects on propeller blade loading, as this is the primary source of vibratory loads on the propeller disk [16]. The chapter includes a summary of the statistical methods used in the analysis of the extracted data. Results and discussions are presented in Chapter III. This includes some of the common errors found in the data files and the actions taken to eradicate these errors. Overall aircraft usage data is presented to describe the commuter airline flight profile and to illustrate the general operation of the BE-1900D, followed by the ground operations data. The data presented includes the restricted shaft speed range operations, use of reverse propeller, and takeoff rotations. This chapter concludes with presentation of the angle of attack and gust loads figures along with the engine and propeller usage numbers. Concluding remarks are presented in Chapter IV.

II. METHOD OF ANALYSIS

A. DIGITAL FLIGHT DATA RECORDER DATA AND FORMAT

The aircraft in this study were fitted with Fairchild F1000 Digital Flight Data Recorders (DFDR). A recording device developed by Systems and Electronics Inc (SEI) was added to the aircraft to allow the information gathered by the DFDR to be stored over a much longer time period for post processing. Raw flight data was extracted and converted into DOS file formats by the airline ground editing station and copied onto hard disks. This editing station also performed an integrity check of the flight data and removed flight sensitive information [8]. The data was received in text file format. The parameters recorded by the DFDR are summarized in Table 3.

Table 3. Recorded flight data parameters

Parameter (Units)	**Sample Rate**	**Units**
Vertical Acceleration	8 Hz	g
Longitudinal Acceleration	4 Hz	g
Pitch Angle	4 Hz	deg
Bank Angle	2 Hz	deg
Pitch Control	2 Hz	deg
Pressure Altitude	1 Hz	ft
Indicated Airspeed	1 Hz	KIAS
Magnetic Heading	1 Hz	deg
RPM (left & right)	1 Hz	RPM
Engine Torque (left & right)	1 Hz	ft-lbf
Prop Reverse (left & right)	1 Hz	discrete
Flap Position	1 Hz	discrete

B. FLIGHT PHASES AND SEPARATION CRITERIA

With each flight cycle, an aircraft goes through distinctly different phases of flight, and each segment produces unique loading conditions on the propeller. Accordingly, flights were separated into a number of different phases identified as either being a major portion of each flight, or one of special interest in terms of propeller loading. Each flight phase was distinguished from the others by certain unique characteristics. The data was divided into two main categories of operation – ground operations and flight operations. These two broad categories were further subdivided into various smaller phases. The methods used for separating each of these phases, as well some of the parameters of interest during each phase, are discussed in the following sections.

1. Ground Operations

The ground operations of the aircraft were subdivided into three categories, the first of which was general ground operations. In the absence of a weight-on-wheel (i.e. squat switch position) recording, the identification of general ground operations came from knowledge of the BE-1900D's landing configuration stalling speed of 84 knots [13]. The only time that the indicated airspeed was recorded as less than 84 knots was when the aircraft were on the ground. Therefore, the only criterion necessary for the identification of general ground operations was an indicated airspeed of less than 84 knots. One of the issues of interest here was the stabilized operation within the restricted propeller shaft speed ranges. Stabilized ground operation is prohibited in the shaft speed ranges of 400 to 950 RPM and 1250 to 1395 RPM. The reason for these restrictions is not clear, but they could possibly be there to avoid the excitation of resonance frequencies in the propeller, engine, or airframe. Other issues considered during

general ground operations were the time to transition through the restricted shaft speed bands as well as the stabilized shaft speed before engine shutdown.

The remaining two ground operations that did not fall under the general category were reverse cycles and takeoff rolls. The primary purpose of reverse thrust is to aid in the braking of the airplane during a landing rollout, but this function is also used for braking while taxiing and maneuvering on the ground. Since reverse cycles occur during the landing rollout where the airspeed might be greater than 84 knots (i.e. immediately after touchdown), this event could not be considered part of the general ground operations. Selection of reverse thrust while in flight is a very unlikely event as the propeller governors on the BE-1900D employ flight idle stops [17]. Due to these factors, the identification of this ground operation only required the use of the reverse propeller parameter. The parameters of interest during propeller reversals were the airspeed, propeller shaft speed, and engine torque at which this event occurred, as well as the duration of this event.

The final ground operation – the takeoff roll – was identified using the indicated airspeed. For the majority of ground operations, the indicated airspeed was observed to have been recorded in the data files as less than 50 knots. In most cases, the airspeed exceeded 50 knots during flight, landing rollout, or takeoff roll only. Therefore, the point where the airspeed exceeded 50 knots with an increasing trend was called the start of the takeoff roll. The end of the takeoff roll occurred either at liftoff, or upon a decrease in airspeed. The point of interest during the takeoff roll was the takeoff rotation since this was identified as one of the most critical phases of flight in terms of cyclic loading on the propeller disk. Figure 3 shows the typical loading a propeller experiences during a Ground-Air-Ground (GAG) cycle. As can be seen in this figure, the greatest blade stress during a GAG cycle occurs during takeoff rotation. The

parameters studied at takeoff rotation included the airspeed, engine torque, propeller shaft speed, aircraft angle of attack, and the wing upwash angle. The criteria used for the identification of the three ground operation categories are summarized in Table 4.

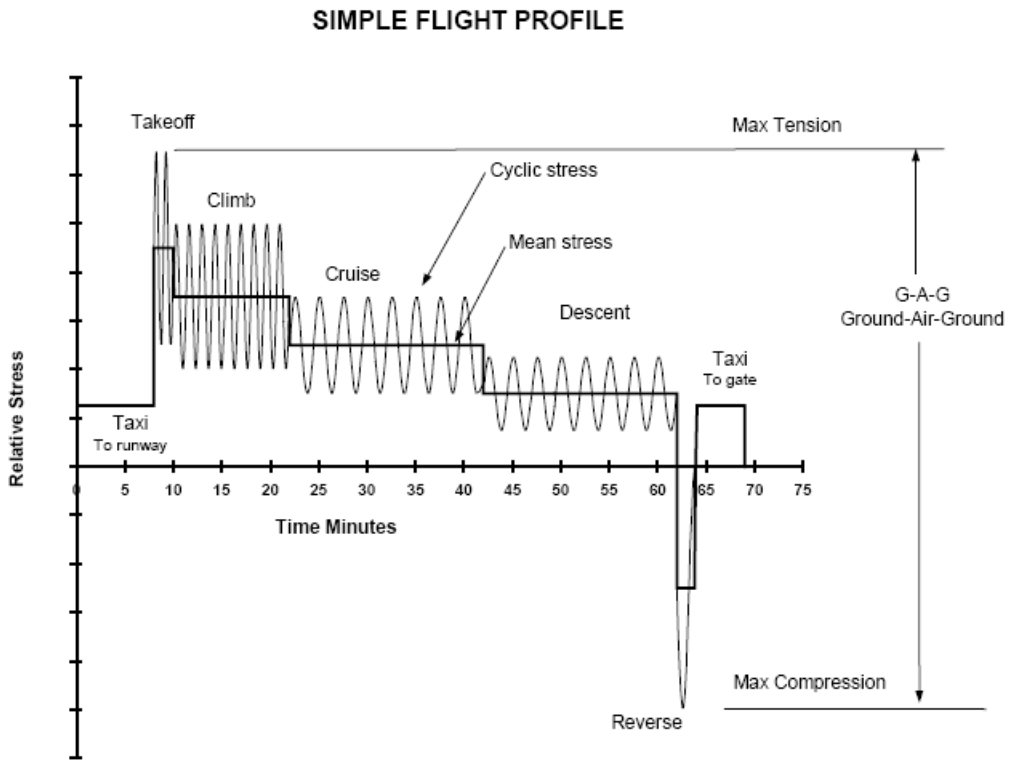

Figure 3. Representation of the vibratory stress cycles for each flight (for illustrative purposes only) [16]

Table 4. Summary of criteria used for the identification of the ground phases

Phase	**Starting Criteria**	**End Criteria**
General Ground Operations	IAS < 84 kts	IAS > 84 kts
Takeoff Roll	IAS > 50 kts AND increasing	Liftoff OR IAS decreases
Reverse Propeller	Reverse parameter indicates propeller in reverse	Reverse parameter indicates propeller not in reverse

2. Flight Operations

Flight operations were divided into five phases – departure, climb, cruise, descent, and approach. A schematic of the five flight phases is presented in Figure 4.

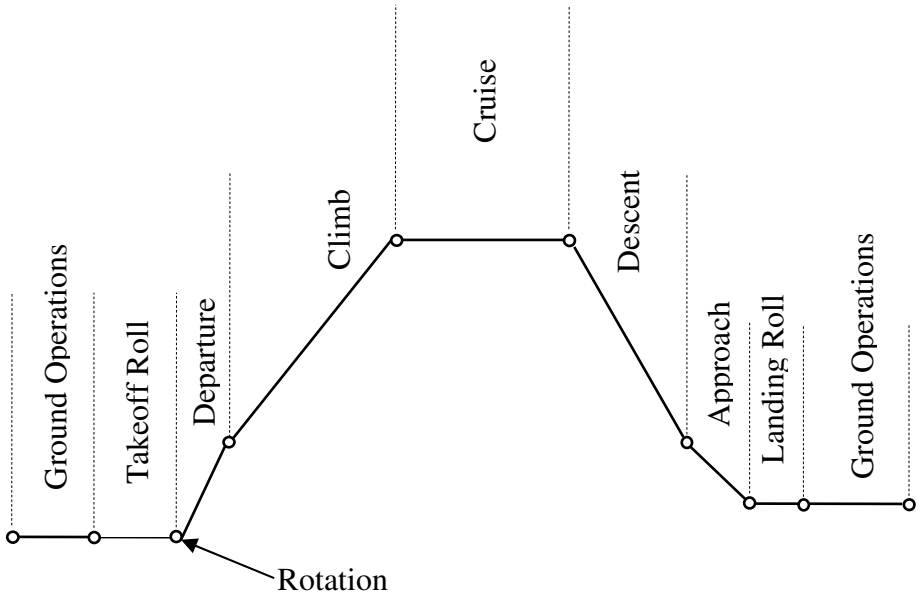

Figure 4. Schematic of the flight phases

A requirement for the departure and approach phases was that the flaps had to be in an extended position. Thus the departure phase started immediately after the takeoff rotation if the flaps were extended. Since a departure segment typically is characterized by a positive rate of climb, in the few cases where flaps were not used for takeoff, the climb phase would commence very shortly after the takeoff rotation. A flap retraction marked the end of this phase. Approach started when the flaps were deployed at an indicated airspeed greater than 101 knots. The aircraft has a stalling speed of 101 knots with the gear and flaps retracted, and since a weight-on-wheel parameter was not recorded, the 101 knots airspeed helped to ensure the aircraft was in the air at flap deployment [13]. The end of approach occurred when the indicated airspeed

decreased to less than 84 knots – indicating a landing – or upon the retraction of the flaps as would occur during a go-around procedure.

Climb, cruise, and descent were distinguished from one another by the vertical speed of the aircraft. Vertical speed was not a recorded parameter and therefore had to be derived from the time history of the altitude data. For these three segments of flight, the flaps had to be in the retracted position and the indicated airspeed above 101 knots to ensure the aircraft was in the air and not in the departure or approach flight phases.

The start of a climb phase was characterized by a rate of climb greater than 750 FPM for 20 seconds. The end of climb was marked when the vertical speed decreased below 750 FPM for 20 seconds. When the vertical speed value remained within ±200 feet per minute for 20 seconds, the cruise segment started. The average altitude during the first 20 seconds of a cruise was used to determine the termination point of this phase. When the difference between this average value and the altitude of the aircraft remained greater than 250 feet for at least 20 seconds, the cruise segment ended. A rate of descent that remained greater than 750 FPM for 20 seconds marked the start of a descent phase. Unlike a climb segment, this phase required multiple ending criteria as this phase could be followed either by a cruise, an approach, or possibly even a landing without flaps. To account for the three possible scenarios, this phase was terminated if either the rate of descent was below 750 FPM for 20 seconds, the flaps were deployed and remained extended for 20 seconds, or if the airspeed remained below 101 knots for 20 seconds. The separation criteria used for the five flight phases are summarized in Table 5.

Table 5. Summary of criteria used in the identification of the five flight phases

Phase	Start Criteria	End Criteria
Departure	Takeoff rotation AND flaps extended	Flap retraction
Climb	VS > 750 FPM for 20 s (flaps up; IAS > 101 kts)	VS < 750 FPM for 20 s
Cruise	|VS| ≤ 200 FPM for 20 s (flaps up; IAS > 101 kts)	Δh > 250 ft for 20 s from average altitude of first 20 s of cruise
Descent	VS < -750 FPM for 20 s (flaps up; IAS > 101 kts)	VS > -750 FPM for 20 s OR flaps extended for 20 s OR IAS < 101 kts for 20 s
Approach	Flap extension at IAS > 101 kts	IAS < 84 kts OR flap retraction

C. METHODS OF DATA EXTRACTION

1. Ground Operations

a) Operation within Prohibited Propeller Shaft Speed Ranges

While on the ground, stabilized operation within propeller shaft speed ranges from 400-950 RPM and 1250-1395 RPM is prohibited. When the shaft speed was within one of these ranges, the amount of time it remained within that range was recorded. All of the recorded times greater than 5 seconds were added together to get the total time the propellers were operated in the restricted zones for more than 5 seconds. The same was done for periods greater than 10, 15, 20, 25, and 30 seconds respectively. The reason for the different time cut-offs was because the restricted shaft speed statement did not define the length of time required for an operation within one of these bands to be considered stabilized. The total time accumulated while operating the

propeller within the prohibited ground operation zones was found by adding all the saved times. This value was extracted for the purpose of comparing it to the time values discussed above.

During normal operations, the propeller shaft speed has to transition through these restricted bands, and therefore the duration of the transitions through these ranges was of interest. A transition was defined to occur when the shaft speed either increased or decreased through one of these bands. If the shaft speed entered and exited a band from the same side, it was not considered to be a transition. The absence of a clear definition of "stabilized operation" came into play again with the restricted zone transitions. There were cases where a slow transition through one of these ranges was counted as a stabilized operation due to its total duration. A 60s time limit was used as a maximum duration for transitions. Transitions characterized by increasing shaft speeds were separated from those with decreasing shaft speeds.

b) Propeller Shaft Speed before Engine Shutdown

One of the characteristics of the recorded engine data was that the propeller shaft speed assumed a negative value when the engine was not running. The shaft speed at idle was observed in the data files to remain around 1000 RPM and when a shutdown occurred plummeted to a negative value. Accordingly, this parameter was found by first locating a point in a data file where the shaft speed took on a negative value. The shaft speed at a point where the difference between two consecutively recorded values was less than 20 RPM shortly before the negative value point was called the shaft speed before engine shutdown.

c) Reverse Propeller

Throughout a flight, the propellers are required to produce thrust in the direction of travel, except upon landing and during ground maneuvering. During these stages of operation where reverse thrust is used, the propellers are loaded in a direction opposite to the loading they experience during the majority of operation. Figure 3 illustrates this opposite axial loading clearly. In addition, the potential for propeller flutter during propeller reversal and high power ground operations is also at its highest [16]. Due to these factors, the reverse cycle is an important part of the propeller loading spectrum in terms of fatigue life and flutter potential [16, 18].

Factors that influence the severity of the loads on the propeller during a reverse cycle are the engine torque, propeller shaft speed, and the airspeed at which this event occurs. Propeller reversal was recorded as a discrete parameter in the data files. When this parameter indicated that the propeller was in reverse, the maximum and minimum shaft speed and engine torque during this phase were recorded. The indicated airspeed at the start of a propeller reversal and the duration of the reverse cycle were saved as well.

d) Takeoff Rotation

Identification of the takeoff rotation followed from that of the takeoff roll. The pitch attitude was averaged over the takeoff roll, and a change of more than 2 degrees from the average value was labeled as the point of takeoff rotation. This was not necessarily the point of liftoff, but rather the point where the rotation for takeoff was initiated. In the few seconds following this rotation, the maximum angle of attack, and accordingly the greatest inflow angle into the propeller disk, would be reached. Accordingly, the point of maximum angle of attack within the ten seconds after the takeoff rotation was called the point of liftoff. At the liftoff point the

aircraft might have been a few feet of the ground, but this point would coincide with the maximum inflow angle and was thus of interest. This large inflow angle would lead to the highest once-per-revolution (1P) loads on the propeller blades.

2. Flight Operations

a) Flap Operations

A change in the wing flap position results in a change in the upwash angle ahead of the wing as well as a change in the aircraft angle of attack. The upwash angle arises from the curvature of the streamlines upstream of a lifting system. These changes affect the propeller inflow angle and consequently the 1P loads on the propeller blades. Flap operations at high power settings were of particular interest as the loads on the propellers were already high, and a change in inflow angle would have a more pronounced effect on blade loading. Generally, high power settings were used during takeoff, departure, and go-around, when the flaps would only be retracted from an initially deployed position.

The only parameter studied was the airspeed at which flap retraction occurred. The BE-1900D has three flap positions – up (0º), approach (17.5º), and down (35º) – and the stalling speed of the aircraft with flaps in the respective positions is 101, 90, and 84 knots [13, 17]. When the flap position indicator changed from down to approach at airspeeds greater than 90 knots, or from approach or down to up at airspeeds above 101 knots, a flap retraction was assumed. The flaps had to be in one position for three seconds before retraction and then remain in the new position for another three seconds for the operation to be considered a flap retraction. The three second time limit eliminated erroneous flap position readings that occurred randomly in some of the data files. The airspeed limits ensured the aircraft was in the air when the

retraction occurred. Once the change in flap position was determined to be a valid retraction, the indicated airspeed at which the flap retraction occurred was saved.

b) Torque and Thrust Correlated with Propeller Shaft Speed

The maximum torque the PT6A-67D engine can produce is 3950 ft-lbf, and 100% propeller shaft speed is equal to 1700 RPM [17]. To obtain the in-flight torque versus propeller shaft speed data, the torque was divided into 20 bands, 18 of which were equally sized between 0 and 3600 ft-lbf. The next band spanned from 3600 to 3750 ft-lbf, and the final band included all torques greater than 3750 ft-lbf. The maximum continuous power limit on the engines on the BE-1900D is 3750 ft-lbf, and operation at torque levels greater than 3750 ft-lbf (takeoff power) is limited to 5 minutes [17]. Therefore, the final two bands were sized to include the maximum continuous power limit. Propeller shaft speed was also separated into 20 bands between 800 and 1800 RPM. The maximum of 1800 RPM was used since this parameter was regularly observed to be between 1700 and 1800 RPM during high power operations (i.e. takeoffs). Another reason for this upper limit was the maximum propeller over-speed limit of 110%, or 1870 RPM, which meant shaft speeds greater than 1700 RPM were possible [17]. Whenever a combination of a torque and shaft speed band occurred, that combination was incremented by one. In essence, the number of occurrences of each torque and shaft speed combination was found. Knowing each occurrence lasted one second, the number of occurrences was then converted to a percentage of the total flight time.

Performance maps provided by Hartzell Propeller Inc were used to find the thrust versus propeller shaft speed while in flight. The thrust generated by the propellers had to be extracted from these maps using the shaft speed, torque, true airspeed, and pressure altitude. Since outside

air temperature was not a recorded parameter, standard atmospheric conditions were assumed and used along with pressure altitude to estimate the local air density, ρ_∞, from Equation 1 [8].

$$\rho_\infty = \rho_{ISA}\left(1 - 6.879 \cdot 10^{-6} \cdot H\right)^{4.256} \tag{1}$$

The recorded indicated airspeed could then be converted into true airspeed using Equation 2.

$$TAS = IAS\sqrt{\frac{\rho_{ISA}}{\rho_\infty}} \tag{2}$$

Maps for various propeller tip Mach numbers were provided. The thrust coefficient of this propeller was mapped in the propeller performance maps as a function of power coefficient and advance ratio. These quantities are defined in Equations 3 through 5 [19].

$$J = \frac{V_T}{nD} \tag{3}$$

$$C_p = \frac{P}{\rho_\infty n^3 D^5} \tag{4}$$

$$M_{tip} = M_\infty\sqrt{1 + \left(\frac{\pi}{J}\right)^2} \tag{5}$$

The advance ratio was simply a function of true airspeed and propeller shaft speed. Power was determined from the product of the torque and the propeller shaft speed. The propeller tip Mach number was a function of the free stream Mach number and the advance ratio. The free stream Mach number was determined from the ratio of the aircraft true airspeed to the local speed of sound. The speed of sound at a given pressure altitude was computed using Equation 6, and the free stream Mach number was then found using Equation 7 [8].

$$a = a_0\sqrt{\left(1 - 6.876 \cdot 10^{-6} \cdot H_p\right)} \tag{6}$$

$$M_\infty = \frac{V_T}{a} \tag{7}$$

The thrust coefficient, defined in Equation 8, was extracted from the performance maps by interpolating between the C_p, J, and M_{tip} values.

$$C_T = \frac{T}{\rho_\infty n^3 D^4} \tag{8}$$

The propeller shaft speed was again divided into 20 bands between 800 and 1800 RPM, and the thrust separated into 17 bands of equal width between 0 and 3400 lbf, and one band that included all thrusts greater than 3400 lbf. Similar to the torque versus shaft speed data, the number of occurrences of thrust and shaft speed combinations were obtained and converted to percentages of the total flight time.

c) Time Versus Airspeed and Torque

The time spent operating at various airspeed and torque levels was examined to understand the basic operation of the aircraft. Indicated airspeed was grouped into bands sized 20 knots wide between 100 and 260 knots; a ninth band spanned from 84 to 100 knots to account for the aircraft stalling speed. The torque was divided into bands between 0 and 3200 ft-lbf with band widths of 400 ft-lbf. Two final bands of unequal size were used again to include the maximum continuous torque limit of 3750 ft-lbf. The number of occurrences of each band was counted, and since indicated airspeed and engine torque was recorded at 1 Hz, each occurrence corresponded to one second at that airspeed or torque level. Thus the number of occurrences matched directly to the total number of seconds spent operating within each band.

d) Angle of Attack

The angle of attack was estimated from a flight dynamics approach, and extracted from the difference between the pitch attitude and the flight path angle. The zero lift line of the aircraft

was assumed to be coincident with a zero degree pitch attitude. However, due to inconsistencies between the data files of the recorded pitch attitude while on the ground, the zero degree pitch attitude was set equal to the average attitude during the takeoff roll. Accordingly all in flight pitch angles used in the estimation of the angle of attack were referenced to the takeoff roll average. This resulted in the takeoff roll angle of attack also being equal to zero degrees since there was no flight path angle on the ground. Flight path angle was calculated from the vertical speed and true airspeed of the airplane. Vertical speed, however, was not a recorded parameter, and had to be extracted from the time history of filtered pressure altitude data. Filtering of the altitude data was necessary due to the presence of noise in this parameter. The altitude was filtered using a running average of its values as shown in Equation 9.

$$H_{i,filtered} = \frac{\sum_{j-4}^{j+5} H_{i+j}}{10} \tag{9}$$

Since the pressure altitude was recorded at 1 Hz, the vertical speed was simply the difference between every two consecutive filtered values. The flight path angle, γ, was then found using Equation 10.

$$\gamma = \sin^{-1}\left(\frac{V_V}{V_T}\right) \tag{10}$$

To account for the pitch attitude being recorded at 4 Hz, the average value of this parameter for each second was used in the calculation of the angle of attack. The angle of attack, α, is given in Equation 11.

$$\alpha = \theta - \gamma \tag{11}$$

In the absence of information on the aircraft's weight and lift coefficient data, this approximation of the angle of attack had to be used. This method is limited to rectilinear flight

with the wings level as maneuvers tend to either increase or decrease the aircraft's g-loading and accordingly the angle of attack. Therefore, the angle of attack was computed only for bank angles less than 5 degrees.

The cumulative occurrences of the angle of attack per 1000 hours and per nautical mile during each of the five flight phases were then determined.

e) Derived Gust Velocity and Change in Inflow Angle

The turbulence that an aircraft experiences during flight is reflected in the recorded normal accelerations data. From this data, the gust velocities associated with the turbulence can be derived. The method used for deriving the gust velocity was the same as that discussed in reference 8. The derived gust velocity, U_{de}, was computed from the incremental normal accelerations using Equation 12.

$$U_{de} = \frac{\Delta n_z}{\overline{C}} \tag{12}$$

The normal acceleration, n_z, was recorded in units of g's, and during steady level flight, the expected mean acceleration was 1g. Typically some offset from the expected mean was present in the accelerations data, and the magnitude of this offset was determined from the average n_z of the first 20 seconds of ground operations before takeoff. The Δn_z parameter then equaled the difference between the expected mean (1g) and the offset corrected n_z values. The quantity $\overline{C}$ is the aircraft response factor and was calculated from Equation 13. The gust alleviation factor, K_g, is defined in Equation 14, and the aircraft mass parameter, μ_g, used in the calculation of K_g is given in Equation 15.

$$\overline{C} = \frac{\rho_{ISA} V_e C_{L_\alpha} S}{2W} K_g \tag{13}$$

$$K_g = \frac{0.88\mu_g}{5.3 + \mu_g} \tag{14}$$

$$\mu_g = \frac{2W}{\rho_\infty g \bar{c} C_{L_\alpha} S} \tag{15}$$

The wing lift-curve slope, C_{L_α}, was obtained from an approximation given in Equation 16 where the wing aspect ratio, A_r, and the Mach correction parameter, β, is defined in Equation 17 and 18 respectively [8].

$$C_{L_\alpha} = \frac{2\pi A_r}{2 + \left(4 + A_r^2 \beta^2 \left(1 + \frac{\tan^2 \Lambda}{\beta^2} \right) \right)^{1/2}} \tag{16}$$

$$A_r = \frac{b^2}{S} \tag{17}$$

$$\beta = \sqrt{1 - M_\infty^2} \tag{18}$$

Aircraft lift-curve slope, C_{L_α}, was assumed to be simply 10% higher than the slope for the wing. Also, since the instantaneous weight was not known, a constant weigh of 16500 pounds was assumed throughout these calculations. The derived gust velocity was calculated for each recorded n_z value and was then converted to the resulting change in propeller blade inflow angle, $\Delta\psi$. This angle is given in Equation 19. A more in depth discussion of propeller inflow angle and its effect on blade loading is given in Section D.1.

$$\Delta\psi = \tan^{-1}\left(\frac{U_{de}}{V_T} \right) \tag{19}$$

An increase or decrease in n_z, however, can either be due to turbulence or flight maneuvers, and thus these needed to be separated from one another. A deadband between ±0.1 degrees from the mean was established to eliminate small changes in the parameters due to the inherent noise in the data. The change in inflow angle within the deadband was considered to be unimportant to the variation in propeller blade loading that it might produce. A $\Delta\psi$ that remained either above or below the deadband for more than 2 seconds was assumed to be due to a maneuver, and anything less than 2 seconds due to a gust. This method of separation of maneuvers and gusts was developed by the University of Dayton Research Institute [8]. When a $\Delta\psi$ was determined to be due to a gust, the maximum $\Delta\psi$ (peak) while above the deadband or minimum $\Delta\psi$ (valley) while below the deadband was determined. The peaks and valleys were then sorted into bins of $\Delta\psi$ that had widths of 0.1 degrees and spanned from -6 to +6 degrees. The number of occurrences of the peaks and valleys was found and categorized according to the flight phase (climb, cruise, or descend) during which they occurred. The number of occurrences was further separated into the altitude bands given in Table 6, with finer divisions at lower altitudes where turbulence is typically more prominent.

Table 6. Pressure altitude bands for $\Delta\psi$ separation

Altitude Bands (feet)
<500
501-1,500
1,501-4,500
4,501-9,500
9,501-14,500
14,501-19,500
19,501-24,500

D. ESTIMATION OF THE WING UPWASH ANGLE

1. Propeller Inflow Angle

One of the largest contributors to the vibratory aerodynamic loads on the propeller is the angle of inflow into the propeller disk. This angle is a combination of the angle of attack, the engine nacelle tilt angle, and the upwash created by the wing. These quantities are shown schematically in Figure 5. Another factor that contributes to the inflow angle that is not shown in Figure 5 is the yaw angle of the airplane. However, this effect was not included in this study since yaw angle was not a recorded parameter. Furthermore, the methods used for determining the angle of attack and the wing upwash angle are limited to flight with the wings level.

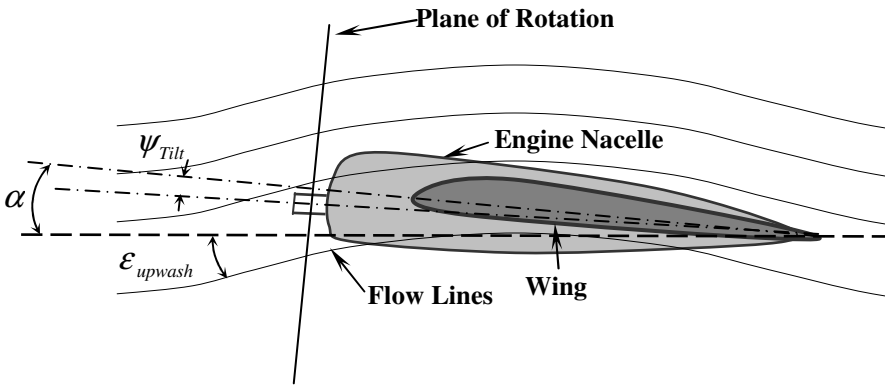

Figure 5. Schematic of the sources of the inflow angle

As a result of the angular inflow into the propeller plane, a downward moving blade will experience a greater angle of attack than an upward moving blade. This creates a difference in the thrust produced by the blade that varies in an *almost* sinusoidal manner as the blade turns. Furthermore, one side of the disk generates more thrust, leading to a yawing moment (P factor). Figure 6 shows a simple representation of a blade cross-section and the components of the airflow velocity a blade element experiences without the inflow angle.

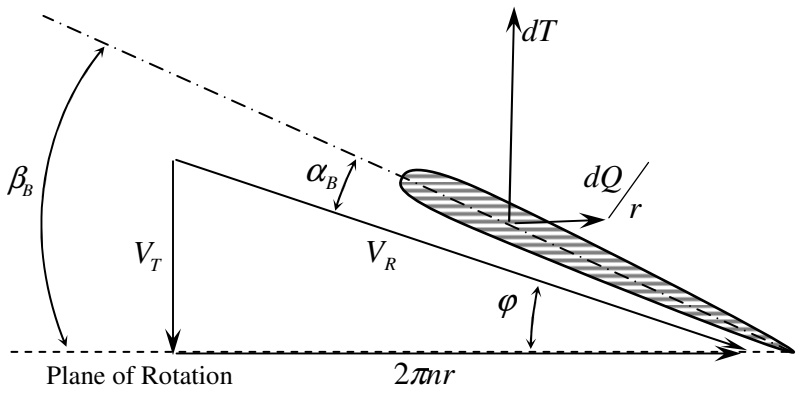

Figure 6. Schematic of forces and velocities acting on a blade element

Airflow entering the propeller disk at an angle can be separated into components that are normal and tangential relative to the plane of rotation. When a blade is moving downward, the tangential velocity of the incoming flow adds to the rotational velocity of the blade, which results in a larger relative velocity, V_R, and a decreased effective pitch angle, φ. Thus the angle of attack of the blade, α_B, increases. The opposite is true for an upward moving blade: the tangential component of the incoming flow subtracts from the rotational velocity, thus decreasing V_R and increasing φ, resulting in a decreased α_B. The increase in V_R and α_B for a downward moving blade results in this blade producing more thrust than an upward moving blade. The outcome of the angular inflow is that each propeller blade experiences a once-per-revolution (1P) loading cycle.

The method used for determining the angle of attack of the aircraft was discussed in the preceding section. The nacelle tilt angle is a geometric property of the airplane and does not require further discussion other than noting that this detailed geometric information of the BE-1900D was not available. A discussion of the method used for estimating the wing upwash angle follows.

2. Equivalent Horseshoe Vortex Method

In this method, the non-uniformly distributed lift along the span is assumed to be generated by a single vortex filament placed at the quarter chord of the wing. The strength of the equivalent horseshoe vortex, Γ_e, is proportional to the weight of the aircraft, which is equal to the lift in non-maneuvering flight as shown in Equation 20.

$$L = W = \rho_\infty V_T \Gamma_e b_e \tag{20}$$

In this equation, b_e is the equivalent wingspan. This quantity is somewhat smaller than the actual span and is a function of how lift is distributed along the span. Assuming this distribution is elliptic, the equivalent and the actual spans are related through Equation 21.

$$b_e = \frac{\pi}{4} b \tag{21}$$

The basic assumptions behind this method are that the equivalent horseshoe vortex generates the same total circulation as does the wing, and the total vortex strength in the wake remains the same as that behind the actual wing. The combination of these allow for determining the equivalent vortex strength and the equivalent span simultaneously, knowing the characteristics of the actual wing. Once these quantities are determined, the Biot-Savart law can be used to estimate the velocities induced by the wing in its vicinity.

3. The Biot-Savart Law

The Biot-Savart law is an electromagnetic equation that relates the intensity of a magnetic field near a current carrying conductor to the magnitude of the current. When this law is applied to aerodynamics, current is equivalent to the vortex strength, and the magnetic field strength equivalent to the induced flow velocity. This law can be used to estimate the induced flow

velocity in the neighborhood of a vortex filament. The Biot-Savart law is given in Equation 22, where the lengths and angles are defined in Figure 7.

$$dv = \frac{\Gamma}{4\pi r^2}\sin(\eta)ds \tag{22}$$

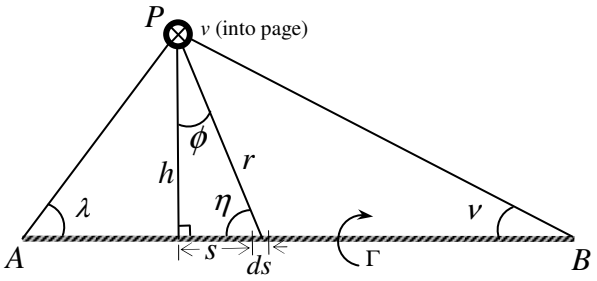

Figure 7. Velocity (v) induced at point a P by a vortex of strength Γ and length AB

In order to find the total velocity induced by the vortex filament at point P, Equation 22 has to be integrated over the length of the vortex filament. From Figure 7 the relations given in Equations 23 through 26, which are needed for integrating Equation 22, can be established.

$$\sin\eta = \cos\phi \tag{23}$$

$$s = h\tan\phi \tag{24}$$

$$r^2 = h^2\sec^2\phi \tag{25}$$

$$ds = h\sec^2\phi d\phi \tag{26}$$

Substituting these relations into Equation 22, the differential induced velocity can be expressed in terms of a single variable, ϕ.

$$dv = \frac{\Gamma}{4\pi h}\cos(\phi)d\phi \tag{27}$$

The limits of the integration of Equation 27 are from point A to point B (Figure 7), which are given in terms of the angle ϕ in Equations 28 and 29.

$$\phi_A = -\left(\frac{\pi}{2} - \lambda\right) \tag{28}$$

$$\phi_B = \left(\frac{\pi}{2} - \nu\right) \tag{29}$$

The result of the integration is given in Equation 30.

$$v = \frac{\Gamma}{4\pi h}(\cos\lambda + \cos\nu) \tag{30}$$

When this equation is applied to a semi-infinite vortex, the angle of the infinite end goes to zero, which then results in Equation 31.

$$v = \frac{\Gamma}{4\pi h}(\cos\lambda + 1) \tag{31}$$

4. Estimation of the Upwash Angle

Using Equations 30 and 31, the upwash velocity generated by the wing at the plane of the propeller was estimated from the aircraft weight and the wing geometry. During takeoff rotation, ground effect was also included using the method of images while it was neglected in other phases of flight.

Detailed dimensions of the BE-1900D, such as the positions of the engine nacelles and the locations of the propeller plane, were not available. Therefore, these dimensions were estimated from the schematic of the aircraft shown in Figure 1. The location of the propeller plane relative to the bound vortex located at the quarter chord of the wing and the trailing vortices, in terms of h, λ, and ν, was needed in the calculation of the upwash velocity. Figure 8 shows the top view of the aircraft with the dimensions used for the subsequent analysis. As indicated in this figure, the upwash was determined at the center of the plane of the propeller (i.e. the base of the spinner).

Three filaments constituted the equivalent horseshoe vortex: two semi-infinite trailing vortices and one bound vortex, all of strength Γ_e. Each vortex contributed to the total upwash velocity. The two trailing vortices induced a downward velocity at the plane of the propeller while the bound vortex induced an upward velocity. The total velocity induced at the plane of the propeller was the sum of the three induced flow velocity vectors. Due to symmetry, the induced velocities were equal in the planes of both propellers.

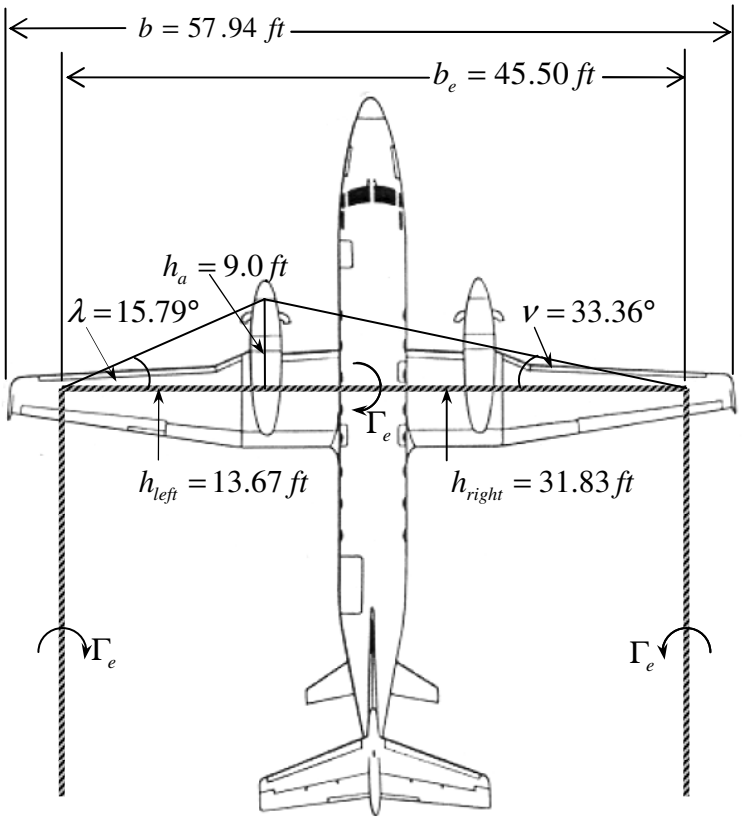

Figure 8. Dimensions of the equivalent horseshoe vortex relative to the propeller planes

Equation 20 can be combined with Equations 30 and 31, to determine the induced velocity in terms of three variables: aircraft weight, airspeed, and air density. The combination is given in Equation 32.

$$v = \frac{W}{4\pi\rho_\infty V_T b_e}\left\{\frac{1}{h_a}(\cos\lambda + \cos\nu) - \frac{1}{h_{left}}(1-\sin\lambda) - \frac{1}{h_{right}}(1-\sin\nu)\right\} \tag{32}$$

After determining the upwash velocity at the plane of the propeller, the upwash angle, ε, was found from Equation 33. The schematic of the induced velocity and its relation to the upwash angle is shown in Figure 9.

$$\tan(\varepsilon) = \frac{v}{V_T} \tag{33}$$

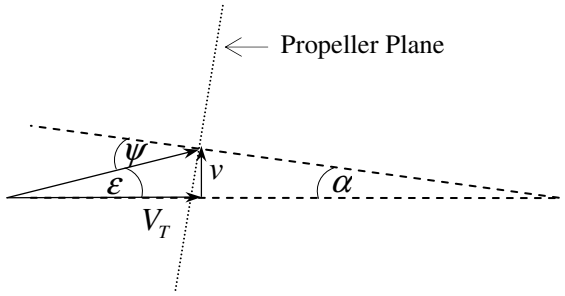

Figure 9. Illustration showing the effect of the upwash velocity on the inflow angle, ψ

The total inflow angle, ψ, is then simply equal to the sum of the angle of attack, α, the upwash angle, ε, and the nacelle tilt angle, ψ_{tilt}, as shown in Equation 34.

$$\psi = \psi_{tilt} + \alpha + \varepsilon \tag{34}$$

5. Special Considerations for Ground Effect

When an aircraft is operated within ground effect, the curvature of the streamlines ahead of the wing is reduced. Thus the amount of upwash produced by a wing within ground effect is less than that of an equivalent wing flying outside of ground effect at the same weight and dynamic pressure.

Ground effect was estimated using the method of images, which is done by placing a horseshoe vortex system under the ground. This vortex system was the mirror image of the equivalent horseshoe vortex on the aircraft. The ground acted as a plane of symmetry between the two vortex systems. The Biot-Savart law was used again in the same fashion as discussed in the preceding section, except in this case different lengths and angles from those shown in Figure 8 had to be used. The lengths and angles now depended on the height of the propeller axis above the ground.

The net effect of the vortex system placed underground was a downward induced flow velocity, and thus the total upwash velocity in ground effect was then given by Equation 35.

$$v_{tot} = v_{upwash} - v_{GE} \tag{35}$$

The effect of the vortex system placed underground became negligible at an altitude above ground level roughly equivalent to the wingspan of the aircraft. Therefore, ground effect was not included in the calculations beyond takeoff rotation.

E. STATISTICAL ANALYSIS

One of the goals of this project was to describe the information contained in the large amount of flight data in statistical form to assist the operators, the regulators, and the manufacturers in better understanding the actual usage of propellers. For some of the parameters considered in this study, representation with a simple normal distribution was not appropriate. For example, a normal distribution would have suggested a negative value of a parameter such as time or torque to be probable when in fact it was physically impossible. To aid in the selection of an appropriate distribution in such cases, the Anderson-Darling (A-D) goodness of fit test was used. This goodness of fit test, which is very similar to the Kolmogorov-Smirnov (K-S) test, is a

method of determining how well a hypothesized distribution fits the distribution of the data set except, the A-D test detects discrepancies in the low-probability regions, which is where many distributions differ [20].

The data for airspeed at the start of a reverse cycle produced a distribution with a double hump. Applying a simple distribution to this data would have resulted in the loss of this unique trend. In cases like this, the investigator's judgment was used to determine the appropriate distribution to describe the data. For this particular case, a bar chart was determined to be a more appropriate representation than a statistical distribution to ensure the preservation of the double hump.

In those cases where duration of an event was of interest, such as time to transition through a restricted shaft speed range, a normal distribution sometimes suggested that a negative time to transition was probable. Figure 10 shows a normal distribution fitted to the time to transition parameter, clearly illustrating this.

Another reason for not using a normal distribution for some parameters was because the A-D goodness of fit test indicated that another distribution fitted the data better. An example of this was the airspeed at flap retraction where a beta distribution was used. For both the flight and ground operations data the Anderson-Darling goodness of fit test often suggested the use of distributions different from those used. The judgment of the investigator was used in such cases. The most important attribute of a distribution was reasoned to be an accurate portrayal of the trends observed in the data. Rather than using distributions the A-D test showed to be slightly better, but not as commonly used, it was decided to use the better known distributions. This ensured that the results of this study could be used without the need for an extensive knowledge

of statistics. Table 7 shows the parameters that required statistical representation, along with the distributions and statistical parameters used to describe each.

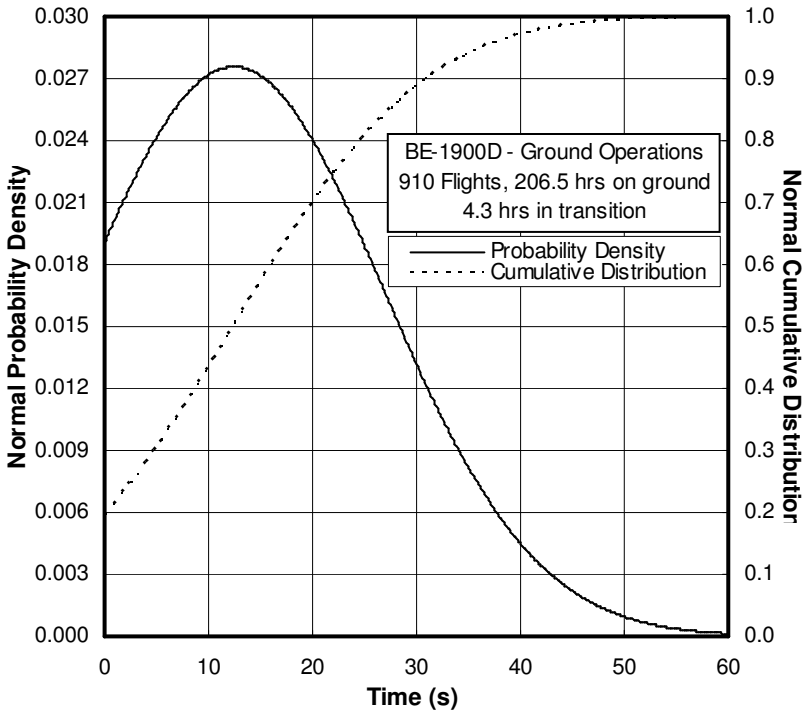

Figure 10. Normal probability density of the time to transition through the restricted RPM ranges (increasing RPM)

Table 7. Summary of distributions used for presentation of aircraft operations data

Parameter	Figure #	Distribution	Statistics
Flap retraction airspeed	13	Beta	a = 120.41, b = 9.447E+7 α_1 = 3.467, α_2 = 1.108E+7
RPM before shutdown	18	Normal	μ = 1015.3 σ = 85.122
Restricted RPM transition (increasing)	20	Lognormal	μ = 2.067 σ = 0.890
Restricted RPM transition (decreasing)	20	Lognormal	*μ = 0.999* *σ = 0.903*
Time in reverse	22	Lognormal	*μ = 1.841* *σ = 1.133*
Maximum RPM during reverse	23	Normal	*μ = 1107.0* *σ = 123.16*

Table 7. Summary of distributions used for presentation of aircraft operations data (continued)

Parameter	Figure #	Distribution	Statistics
Minimum RPM during reverse	23	Normal	μ = 984.32 σ = 119.08
Maximum torque during reverse	24	Lognormal	μ = 6.229 σ = 0.996
Minimum torque during reverse	24	Lognormal	μ = 5.846 σ = 1.063
RPM at rotation	25	Normal	μ = 1725.0 σ = 17.41
Torque at rotation	26	Normal	μ = 3518.0 σ = 195.98
Airspeed at rotation	27	Normal	μ = 112.11 σ = 5.029
Liftoff attack angle (no flaps)	28	Normal	μ = 4.477 σ = 0.655
Liftoff attack angle (approach flaps)	28	Normal	μ = 4.1835 σ = 0.946
Liftoff attack angle (full flaps)	28	Normal	μ = 4.000 σ = 1.121
Liftoff inflow angle (no flaps)	30	Normal	μ = 6.019 σ = 0.657
Liftoff inflow angle (approach flaps)	30	Normal	μ = 6.039 σ = 0.972
Liftoff inflow angle (full flaps)	30	Normal	μ = 5.724 σ = 1.129
No ground effect (approach flaps)	31	Normal	μ = 6.579 σ = 1.040

F. CHAPTER SUMMARY

In Chapter II, the categories of operation were discussed along with comprehensive explanations of the methods used for extracting and analyzing the large volume of flight data contained within the data files. The propeller inflow angle was thoroughly explained, along with the method used to estimate this parameter for the aircraft in this study.

In the following chapter, the results of the examination of the extracted aircraft operations data are presented. Chapter III commences with a brief discussion of the available flight data. This discussion includes some of the common problems found in the data files and the actions taken to eradicate these errors. Overall aircraft usage data is presented to describe the commuter airline flight profile and illustrate the general operation of the BE-1900D. This is followed by the ground operations data. The data presented here includes the restricted shaft speed range operations, use of reverse propeller, and takeoff rotations. The final category of data pertains to flight operations where the angle of attack and gust loads figures are presented along with the engine and propeller usage numbers. The data presentation in Chapter III is accompanied by a discussion of the results.

III. RESULTS AND DISCUSSION

A. AVAILABLE DATA

Flight data from 30 Beech 1900D aircraft was received in text file format – one file for each aircraft and each file containing data from multiple flights. Of the 30 files, three files were completely excluded from the study as some of the recorded parameters in these files were plagued by errors. Some errors were present in a few of the remaining 27 files. These errors were typically not present throughout an entire file, thus only the affected parts of the files had to be excluded from the analysis.

A common error in the data files was an inverted reverse propeller parameter. If a data file contained this error, it persisted throughout the entire file. The reverse parameter indicated a reversal throughout an entire flight. Furthermore, when reverse was indeed used, the data indicated that the propeller came out of reverse. This was obviously opposite to what actually occurred and thus easily recognizable. Files affected by this error could easily be corrected by simply inverting the reverse propeller parameter, resulting in inclusion of these files in the investigation.

Some of the data files were plagued by a non-sequential timing error. Typically, four lines of data would be in sequence, followed by another four lines that would be in sequence with each other, but not with the preceding four lines. This timing error was generally only present for the first few thousand lines of data, but it also occurred in random locations in a few files. Since this error did not affect the data files in their entirety, the affected flights in the files were excluded from the analysis, resulting in the majority of the data from these files being used.

Two out of the three files excluded from the study had incorrectly recorded values of engine torque. This error was identified by comparing the torque values in these two files to the torque values in other files. The third excluded file's flap position parameter was inoperative. The flaps were always recorded as being in the up position except for a second or two at random locations in the file. The affected parameters in these file were important to this study, and thus these could not be included in the analysis.

Overall, the data was of very good quality, and the majority of the data was used in the investigation. Very few errors were present in the 27 files, resulting in the extraction of flight data for 910 flights, representing about 589 flight hours. Table 8 presents the amount of flight and ground hours extracted from each aircraft included in the study as well as the number of flights from each aircraft.

Table 8. Number of flights and hours of operations extracted from the data

Aircraft Number	Number of Flights	Flight Hours	Ground Hours	Aircraft Number	Number of Flights	Flight Hours	Ground Hours
1	30	23.2	7.9	**15**	29	22.0	8.5
2	44	23.0	6.7	**16**	41	20.7	7.8
3	27	20.9	9.2	**17**	34	18.8	7.5
4	32	23.5	6.8	**18**	28	25.5	6.6
5	34	20.3	7.5	**19**	33	22.9	6.9
6	22	14.8	6.2	**20**	25	24.4	6.0
7	34	21.9	7.6	**21**	34	23.3	7.7
8	34	20.9	7.3	**22**	30	17.8	6.8
9	34	21.8	7.7	**23**	23	22.4	9.7
10	42	23.7	7.2	**24**	34	19.4	8.0
11	33	22.2	6.9	**25**	44	20.0	8.3
12	38	22.8	9.2	**26**	39	25.3	7.4
13	41	22.2	8.1	**27**	33	23.0	8.2
14	38	22.5	8.8	**Total**	910	589.1	206.5

B. OVERALL AIRCRAFT USAGE

The purpose of this section is to present data that depicts the usage of the aircraft and some of its systems. Gaining an understanding of the overall usage will aid in the comprehension of the data presented in the following sections. This section does not present data necessarily directly related to the propeller usage and loads, but rather more general operational data. Data such as the individual flight durations, the time spent in the different flight phases, and the flap usage, will be shown in this section.

The first parameter presented here is the flight durations. Figure 11 presents a bar chart of the durations of each flight. The average flight lasted about 39 minutes, indicating the aircraft were not used on long distance flights. Not many flights lasted more than an hour, but a significant number of flights fell within the 5-10 minute range. These short flights could possibly be the result of post maintenance test flights where the aircraft remained within the traffic pattern or even come from short-hop flights from small airports close to a larger one. From the data in this figure, one can derive the average flight distance to be about 150 nautical miles. The short distances flown by these aircraft show the nature of commuter airline flights. Also, these short flight durations mean that these aircraft go through multiple flight cycles much more rapidly than a long haul airliner would. Accordingly, subsystems such as the landing gear, flaps, engines, propellers, as well as the aircraft structure, experience many loading cycles within the operational life of these aircraft. Due to these short cycles, fatigue and wear of the components on these aircraft would be more severe than airliners operated on longer flights.

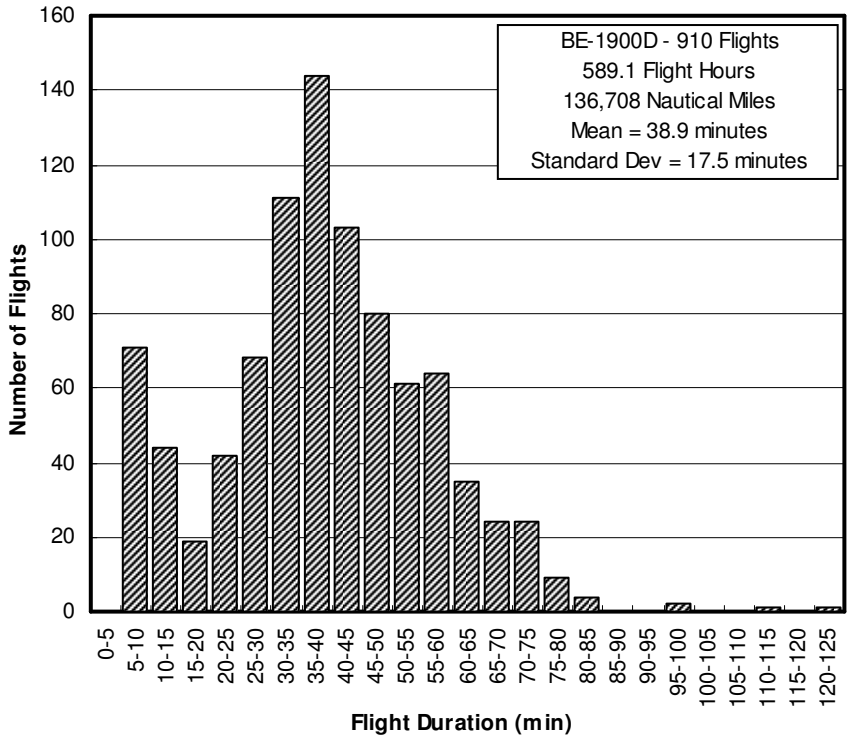

Figure 11. Number of flights versus flight duration

Flap usage is part of both takeoffs and flight operations, and also falls under the usage of an aircraft system category. Accordingly, the flap usage data is presented in this section. Figure 12 shows the percentage of takeoffs and landings performed with the flaps in various positions. The majority of takeoffs were performed with the flaps in the approach position, and only a small percentage of takeoffs were performed with full flaps or no flaps. The reason for using full flaps for takeoff is not clear, but this would potentially decrease the acceleration of the aircraft due to higher drag forces. A takeoff performed without flaps could have been done at airports with longer runways where the aircraft would have been able to accelerate to higher airspeeds before liftoff. Landings were mostly executed with the flaps in the down position, and just a few performed with the flaps in the other two positions. Flaps help to decelerate the aircraft, reduce the stalling speed of the aircraft, lower the pitch angle to aid in forward visibility for the pilots

during the final stages of an approach, and reduce the touchdown speed of the aircraft upon landing. Thus landings with flaps in a position other than down were unanticipated.

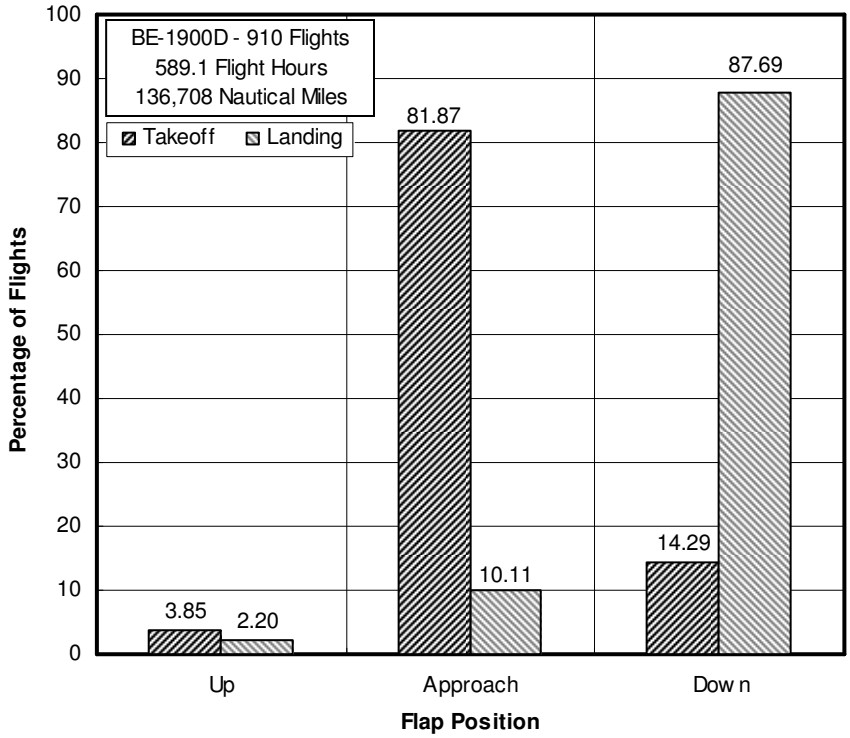

Figure 12. Percentage of takeoffs and landings performed with flaps in the respective positions

Figure 13 shows a Beta distribution of the airspeed at which flap retraction took place. All of the flap retractions occurred at airspeeds greater than 120 knots with an average airspeed of about 145 knots. The maximum flaps extended airspeeds for the approach and down positions are 188 and 154 knots, respectively. A significant number of flap retractions occurred at airspeeds greater than 154 knots, but since the bulk of takeoffs were performed with the flaps in the approach position, the flaps were likely in the approach position at these higher airspeeds. Few retractions occurred at airspeeds greater than 188 knots.

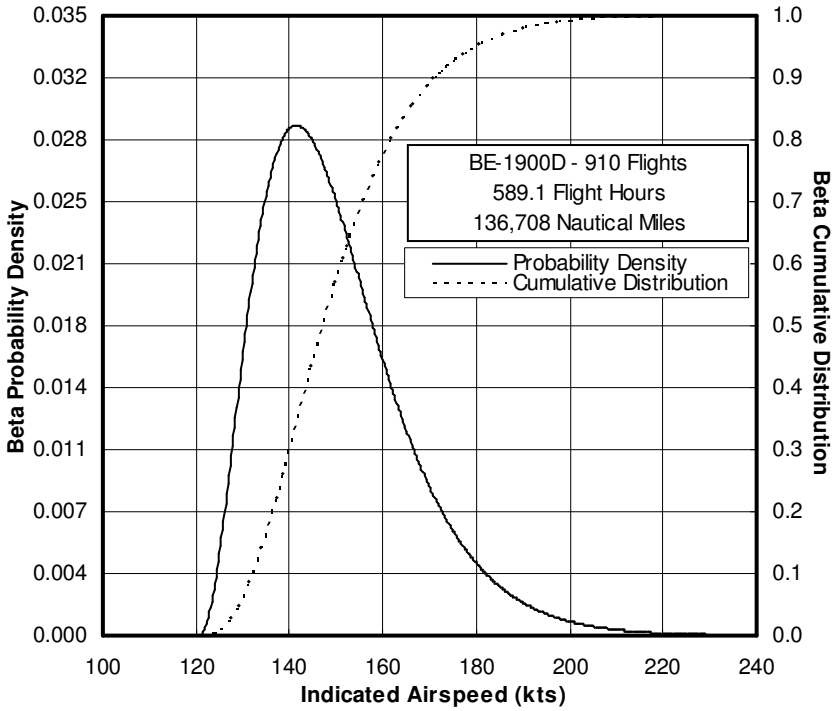

Figure 13. Beta probability density and cumulative distribution of the airspeed at which flap retraction occurs

The percentage of the total flight time with the flaps in the different positions is shown in Figure 14. The flaps spent a small percentage of time in an extended position as would be expected. Departure and approach phases of flight are represented by the flaps in the extended position. Consequently, this figure shows the aircraft spent very little time in departure and approach as compared to the amount of time spent in the climb, cruise, and descent phases. Figure 15, which presents the percentages of the total flight time and flight distance spent within each of the five flight phases, reaffirms what is shown in Figure 14 with regard to flight phase duration. The relation between distance and time for each phase in Figure 15 shows an interesting correlation. Departure, climb, and approach show a smaller distance percentage than time percentage, whereas cruise and descent show a larger distance percentage than time percentage. This figure thus gives information about the airspeed and distance correlation

among the five phases. Cruise and descend were characterized by higher airspeeds than the other three phases, thus the higher distance percentage. The relation between these two flight phases suggests that the cruise airspeed was higher than the descend airspeed. During the final stage of a descent, the aircraft was slowed for flap extension and transition to approach. This means the aircraft would have spent a larger percentage of time at slower airspeeds during descent than during cruise. Departure, climb, and approach were characterized by lower airspeeds, and thus the results seen in Figure 15.

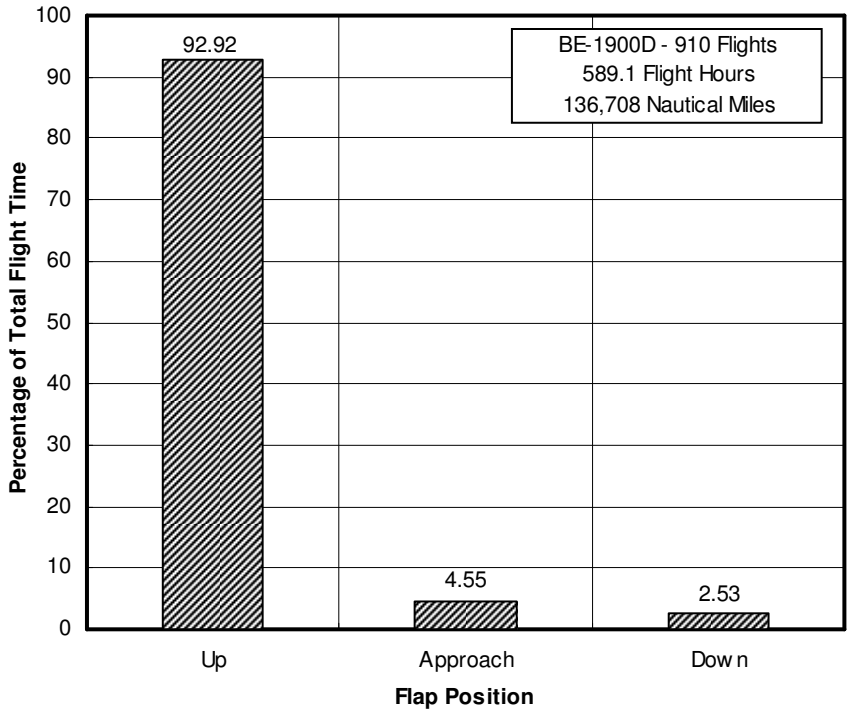

Figure 14. Percentage of total flight time spent with flaps in respective positions

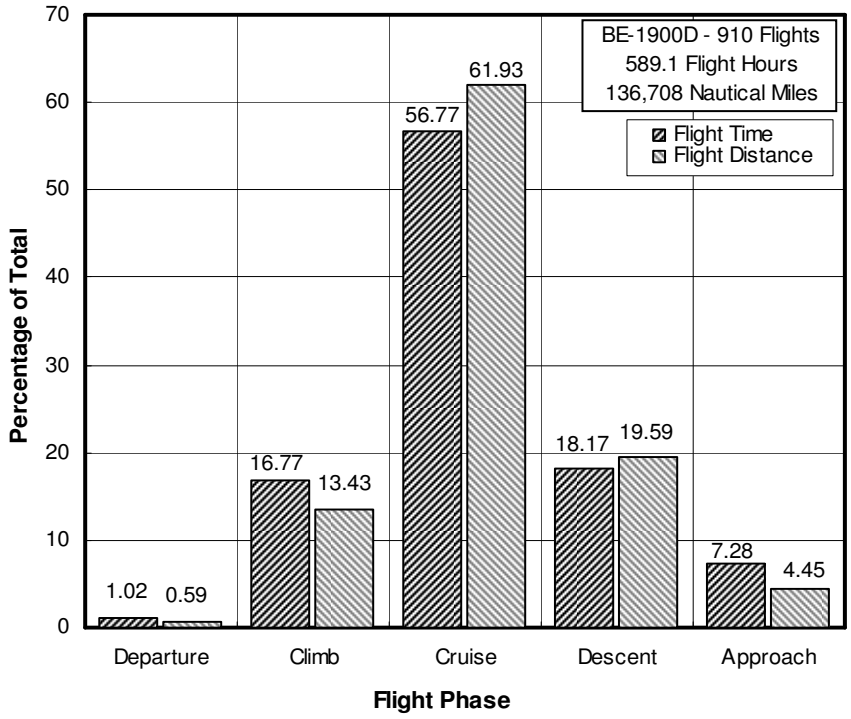

Figure 15. Percentage of total flight time and flight distance spent within each flight phase

The amount of time the engines were operated in different torque bands is shown Figure 16 as a percentage of the total flight time. Only a very small percentage of the flight time was spent at torque levels greater than the maximum continuous limit of 3750 ft-lbf; 0.22 percent of the total flight time is equivalent to about 5 seconds per flight. The vast majority of the flight time was spent between 2800 and 3750 ft-lbf of torque. Similar to Figure 16, Figure 17 shows the percentage of time spent at the different airspeed levels. The aircraft cruised at airspeeds between 200 and 240 knots and maintained airspeeds within this range during descents, thus the large percentage of operation within this range. Rarely did the aircraft exceed the maximum operating speed of 248 knots. The other hump on this figure around the range of 160 to 180 knots is the airspeed at which the aircraft climbed. The data contained within this figure and that in Figure 15 correlate well with one another.

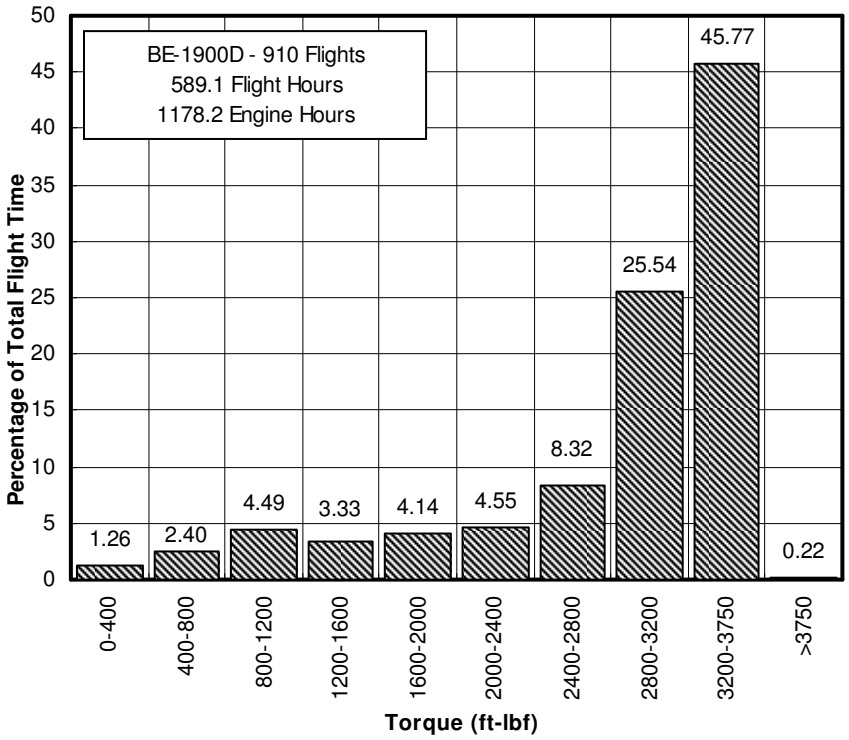

Figure 16. Percentage of total flight time spent operating at different torque levels

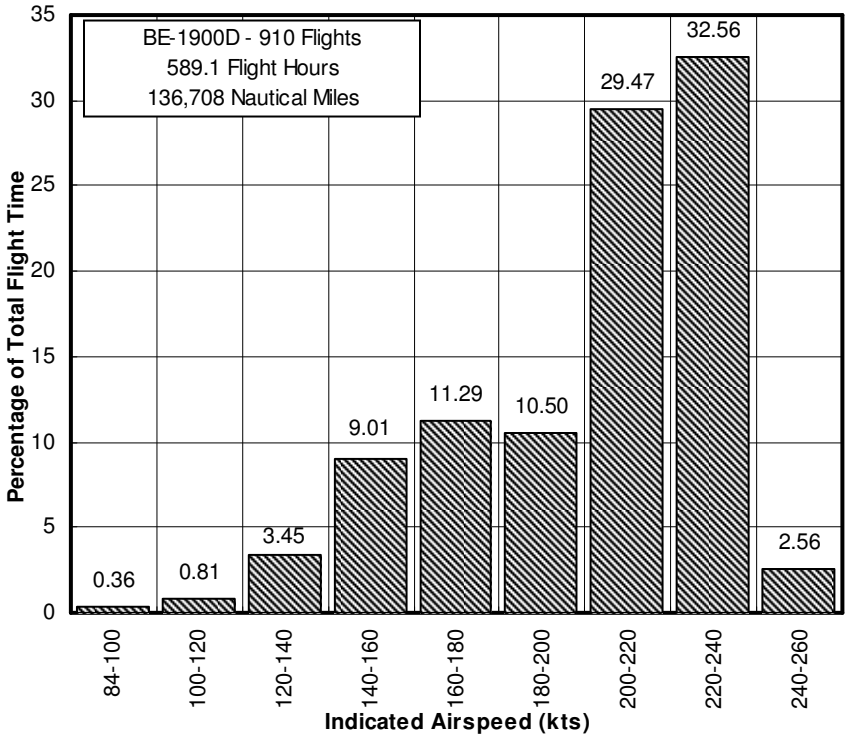

Figure 17. Percentage of total flight time spent operating at different airspeed levels

C. GROUND OPERATIONS

1. General Ground Operations

The parameters studied under the general ground operations category were the propeller shaft speed before engine shutdown, stabilized operations within the restricted propeller shaft speed ranges, and transitions through the restricted ranges.

The first result presented in this section is the propeller shaft speed before engine shutdown and is shown in Figure 18. The idling shaft speed of the propellers is about 1000 RPM and the shaft speed before shutdown fell within a very narrow band around 1000 RPM. A significant number of shutdowns, approximately 20 %, occurred from a shaft speed below 950 RPM, which means the propellers were within a prohibited operating range.

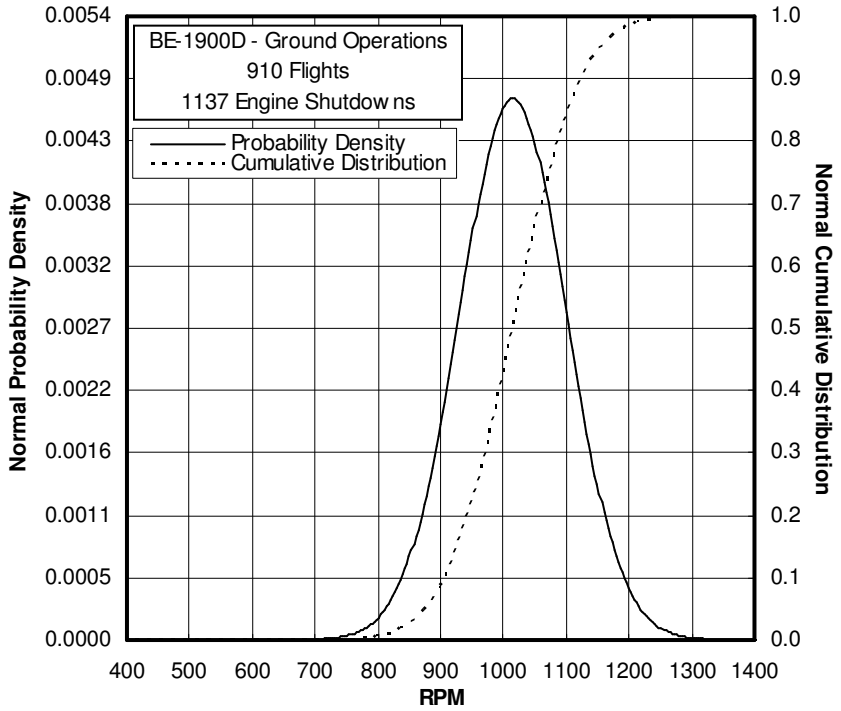

Figure 18. Normal probability density and cumulative distribution of RPM before engine shutdown

Operations within the restricted propeller shaft speed ranges were closely scrutinized. These ranges spanned from 400 to 950 RPM and 1250 to 1395 RPM. Due to the lack of a clear definition of "stabilized ground operations," operations within the prohibited range for various durations are shown in Figure 19. A surprisingly large amount of time was spent within the lower prohibited range, as shown in Figure 19(a). Since a typical idling shaft speed was around 1000 RPM, the propellers were possibly idling just within the lower restricted band. This conclusion is supported by observing that 75% of the total amount of time in the lower restricted band came from being within that range for more than 30 seconds. The result from engine shutdowns, Figure 18, also supports this claim.

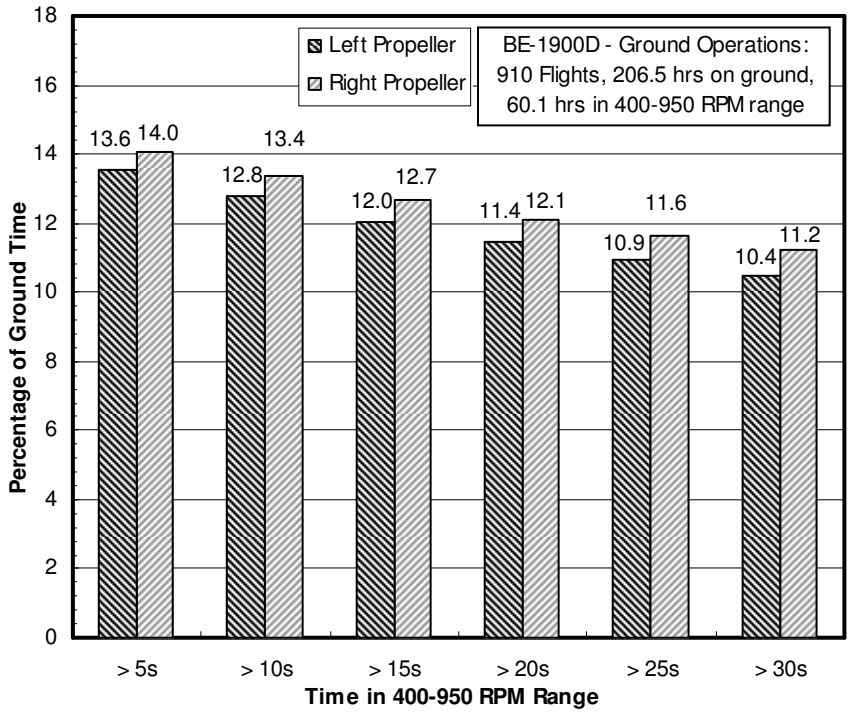

(a) 400 to 950 RPM range

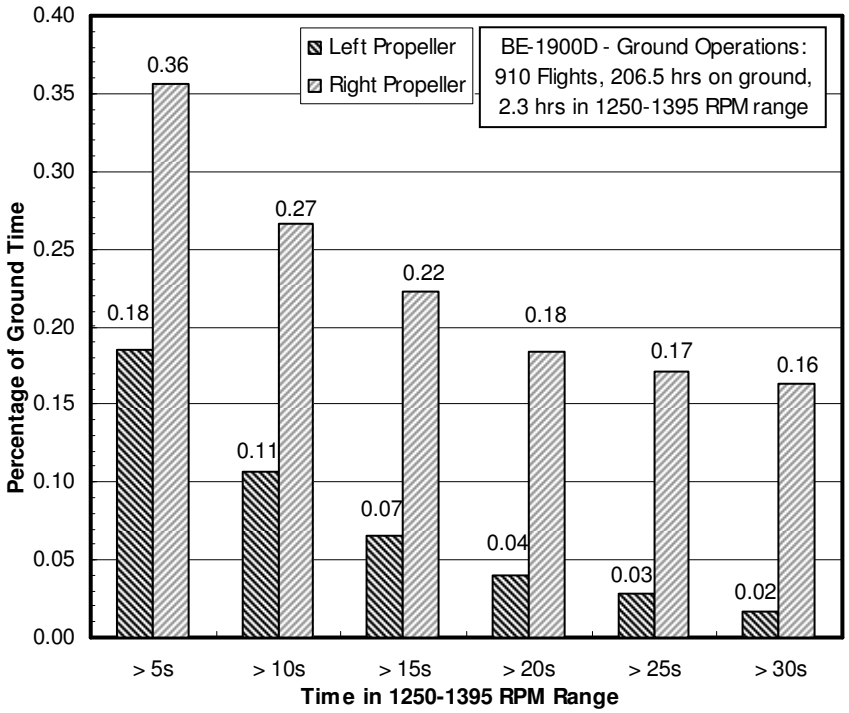

(b) 1250 to 1395 RPM range

Figure 19. Total time spent in the restricted RPM ranges for different time limits

Figure 19(b) show that much less time was spent operating within the upper restricted range. This figure supports the reason given for the large amount of time spent within the lower band as well. The idling shaft speed is well below the upper restricted zone. An interesting characteristic of Figures 19(a) and 19(b) is they both show a smaller amount of time for the left engine than the right. At the end of many flights, only the left engine was shutdown. This was probably done for passenger boarding purposes or for reduced fuel burn by taxiing with one engine. Nevertheless, this operational practice can be seen in Figure 19.

The time to transition through a restricted propeller shaft speed range was studied since these transitions are part of normal operations. Lognormal distributions of the increasing and decreasing shaft speed transitions are shown in Figure 20. The majority of transitions lasted less than 10 seconds. Increasing transitions were generally slower than the decreasing transitions.

This disparity between increasing and decreasing transitions appear to be a valid result when one considers the engine has to overcome aerodynamic drag to increase the shaft speed, whereas the propellers just have to slow with the drag force for decreasing transitions. Many of the transitions are also likely to have been a result of engine shutdowns when the propellers would go into a feathered position because of the loss of oil pressure. This would cause a rapid decreasing propeller shaft speed caused by the very high propeller pitch angle and resulting high drag.

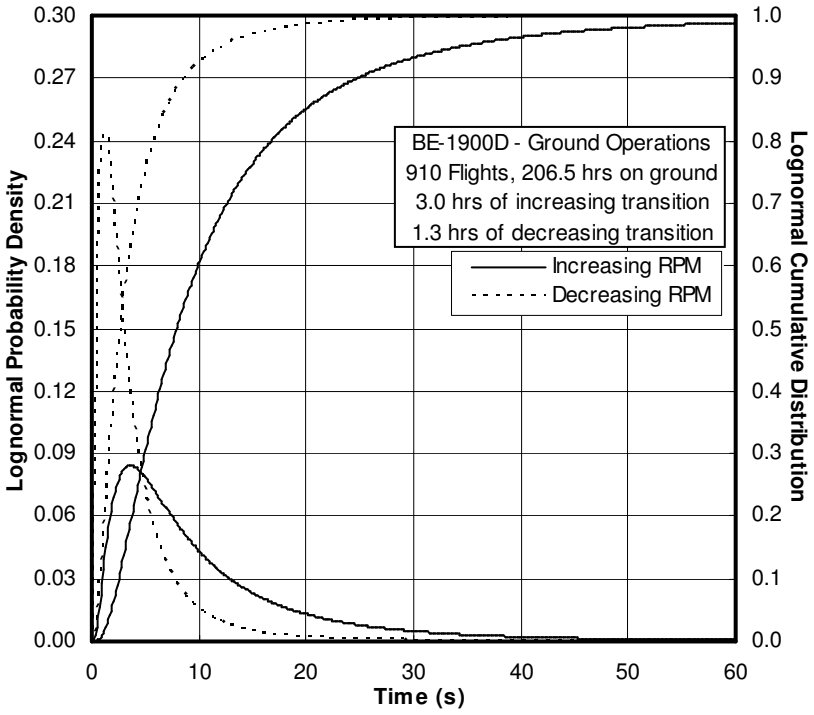

Figure 20. Time per transition through restricted propeller shaft speed ranges

Other than the difference in duration of the two transition types, a contributing factor to the total time difference is the increase of shaft speed at the start of a takeoff run. This transition would have been captured under general ground operations, whereas the decrease of the shaft

speed through the upper prohibited range upon landing would not. During landing, the transition would take place, or at least start, above 84 knots indicated airspeed and thus would not have been captured under the general ground operations.

2. Reverse Propeller

The primary purpose of reverse thrust is for braking during landing. However, as shown in Table 9, reverse thrust was used on only 320 of the 910 landings. It was expected that reverse thrust would have been used during all landings as this would greatly reduce the wear of the wheel brakes and tires. When propeller reversal was used for braking, the reverse parameter regularly indicated that one propeller went into reverse about one to two second before the other. One propeller producing reverse thrust during the landing rollout could result in a very noticeable yawing moment and possible difficulty in directional control after landing. Thus some pilots might have elected not to use reverse for increased passenger comfort. This would be especially true for operations from airports with long runways where hard braking after landing was not necessary.

Table 9. Use of reverse thrust during landing rollout

Landing Reversal	**Number**
Left Propeller	441
Right Propeller	353
Simultaneous	320

The result obtained from extracting the indicated airspeed at the start of the reverse cycle is shown in Figure 21. This figure shows a very interesting double hump – one hump at airspeeds below 50 knots, and another around 80 knots. The minimum recorded airspeed varied from one

data file to the next, but the minimum was always less than 50 knots. Thus the high concentration of reversals at airspeed below 50 knots represents reverse thrust usage during taxi and ground maneuvering. Due to the varying minimum recorded airspeed, the airspeeds below 50 knots in Figure 21 do not represent the true airspeeds of the aircraft at the time of those reversals. The hump on the right was due to reversals during the landing rollout, and as can be seen, this typically occurred at airspeeds between 70 and 90 knots. The total number of reverse cycles (2091) indicated on this figure is the sum of both left and right propeller reversals. In order to compare this figure to Table 9, the number of left and right propeller reversals in Table 9 would have to be added together. From Table 9 and the total number of reversal, approximately 38% of the number of reversals can be seen to have occurred during the landing rollout. This corresponds with the information in Figure 21.

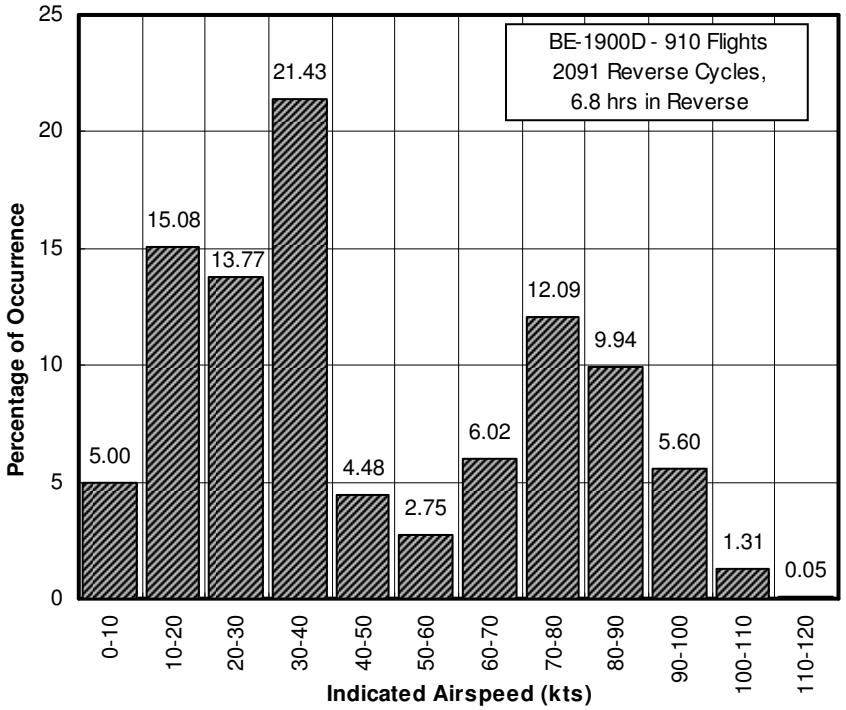

Figure 21. Indicated airspeed at start of reverse cycle

An interesting observation from studying the data files was that reversals of the left and right engine did not necessarily correlate during ground operations. This is postulated to have been done to aid in the ground maneuvering of the aircraft. One propeller producing reverse thrust while the other produces forward thrust would allow the aircraft to make a very small radius turn. In addition, using thrust reversal to turn and brake the aircraft on the ground would decrease brake wear. Reversals upon landing, on the other hand, were usually well correlated between the left and right propellers except for the small time difference at the start of the reversals mentioned earlier.

Figure 22 shows a lognormal distribution of the duration of the reverse cycles. Reversal generally lasted for less than 10 seconds and those lasting longer than 20 seconds occurred very rarely. Reversals upon landing were not expected to last more than 10 seconds as landing rollouts are short duration events. The same was true for reversals while taxiing as reverse thrust would generally be used to brake or turn the airplane and thus be of short duration.

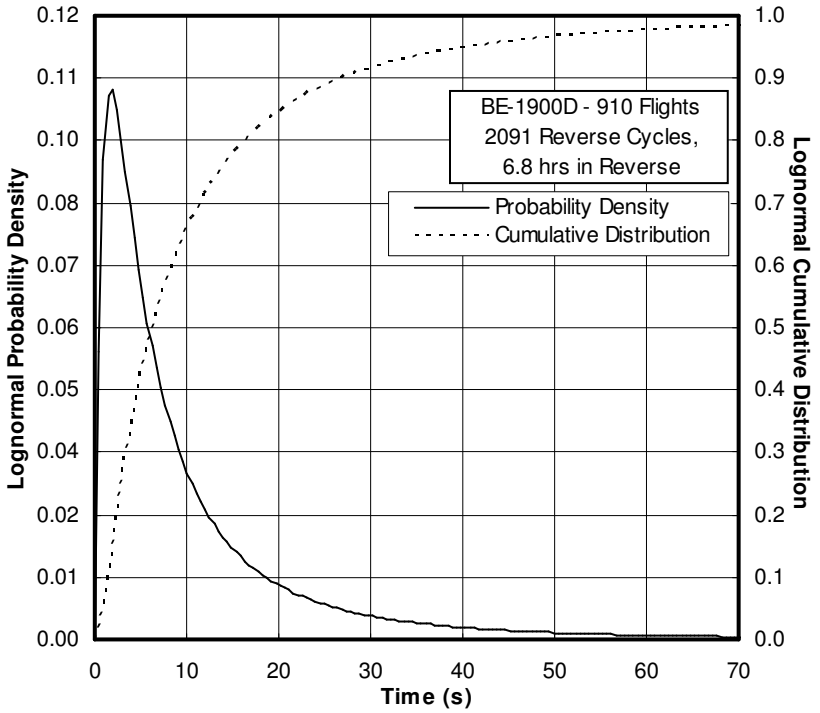

Figure 22. Lognormal probability density and cumulative distribution of the duration of reverse cycles

The last two figures that deal with the reverse cycle, Figure 23 and Figure 24, present the distributions of the maximum and minimum propeller shaft speed and engine torque during a reverse cycle. Figure 23 shows a difference between the maximum and minimum shaft speeds of about 100 RPM and an average reverse propeller shaft speed of about 1050 RPM. The higher shaft speeds shown in this figure are suspected to have come from the landing reversal where the shaft speed was higher due to the faster airflow moving through the propeller disk. The maximum engine torque during a reverse cycle was only slightly higher than the minimum, with the majority of reversals happening with the torque less than 500 ft-lbf. Few reversals occurred with torques greater than 1500 ft-lbf.

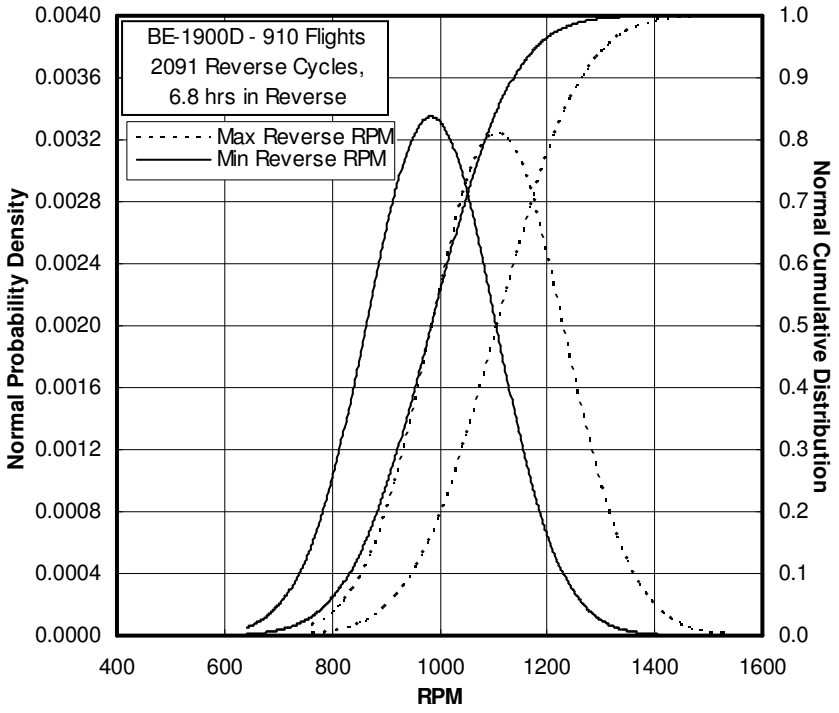

Figure 23. Normal probability density and cumulative distribution of maximum and minimum RPM during reverse cycle

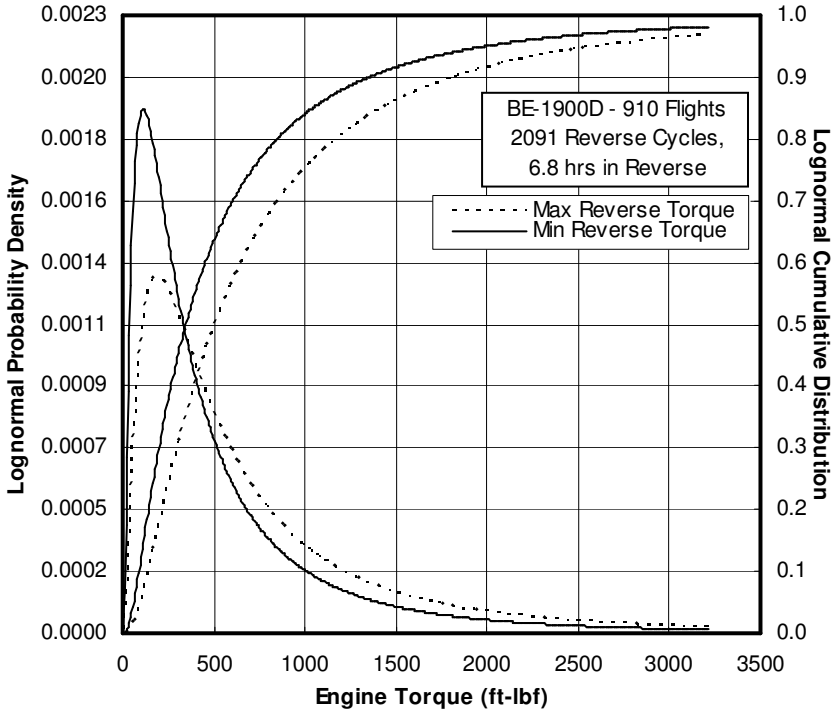

Figure 24. Lognormal probability density and cumulative distribution of maximum and minimum torque during reverse cycle

3. Takeoff Rotation

The takeoff rotation was deemed to be one of the most demanding segments of operation for the propeller blades caused by the high inflow angle coupled with high power settings. Figures 25 and 26 show the propeller shaft speed and engine torque, respectively, at rotation. Full power was generally used for takeoffs, and this can be seen in these two figures that show means of about 1725 RPM and 3500 ft-lbf of torque at rotation. The airspeed at takeoff rotation also affects the severity of the 1P loading the blades experience. This parameter is presented as a normal distribution in Figure 27. Takeoff rotation typically occurred around 112 knots or a dynamic pressure of about 42.5 psf. Rotation does not necessarily correspond with the liftoff point, thus when rotations occurred at lower airspeeds it did not mean the aircraft lifted off the ground at those airspeeds.

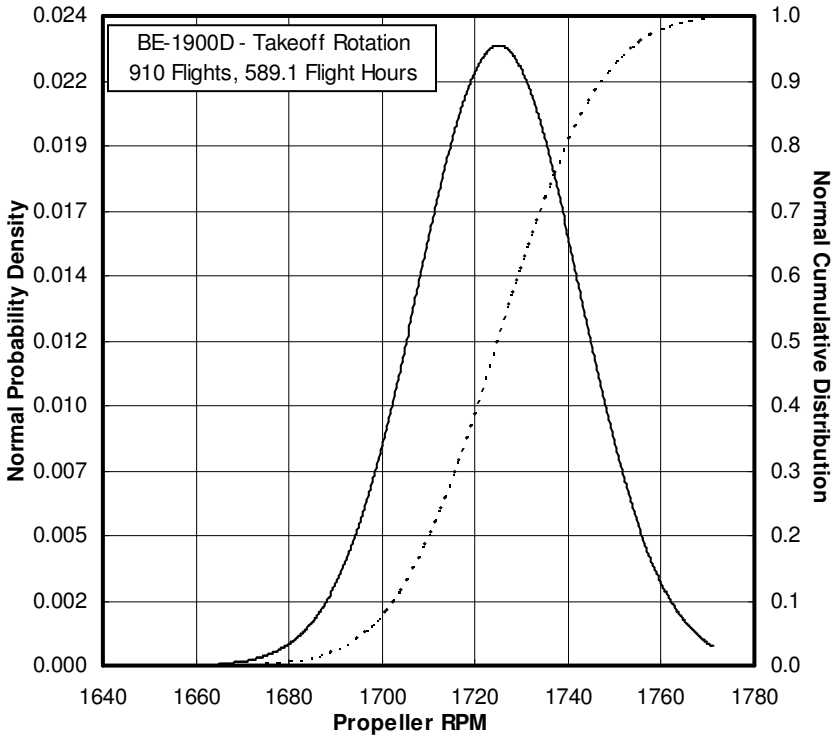

Figure 25. Propeller shaft speed at takeoff rotation

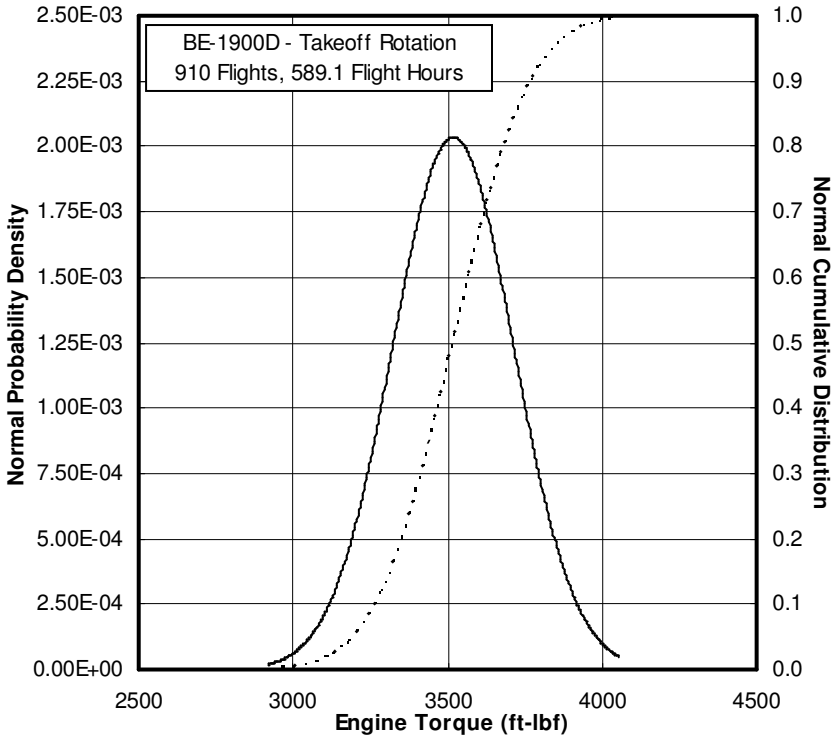

Figure 26. Engine torque at takeoff rotation

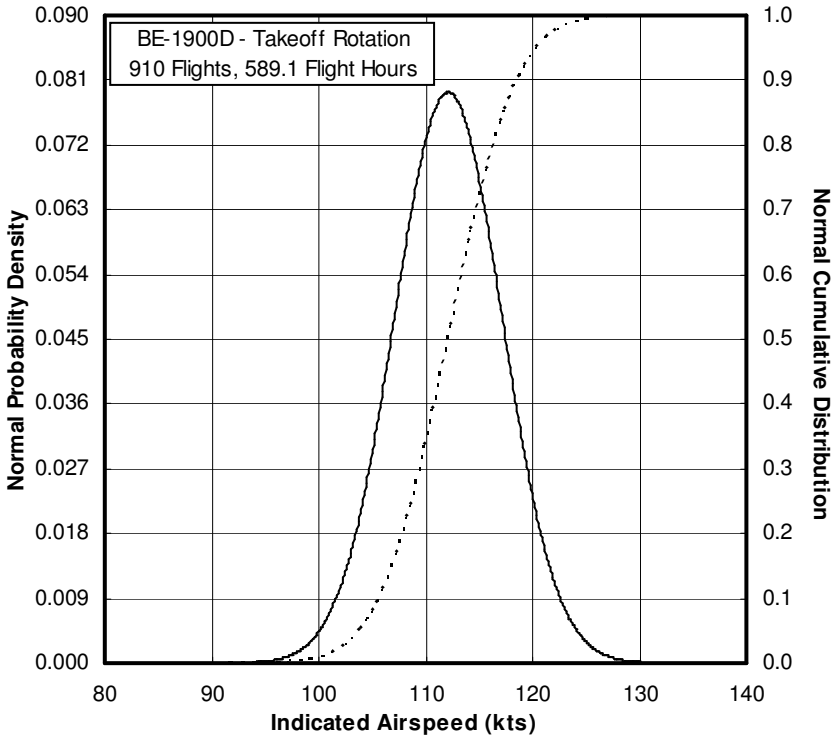

Figure 27. Indicated airspeed at takeoff rotation

The angle of attack at liftoff data is presented in Figure 28. Figure 28(a) shows the normal probability density and Figure 28(b) shows the normal cumulative distribution. Takeoffs were separated by the three flap positions. The average liftoff angle of attack of the takeoffs performed with full flaps was smaller than those with either approach or no flaps. Considering the sample sizes, this result is considered reliable. Approach flaps lessened the liftoff angle of attack from the no flaps case as was expected. However, only 35 no flap cases were extracted in contrast to the 745 approach flap cases, and as a result of the small sample size, the distribution of the no flaps case is considered to be unreliable. A larger number of no flap takeoff cases would have to be studied for conclusive and reliable results.

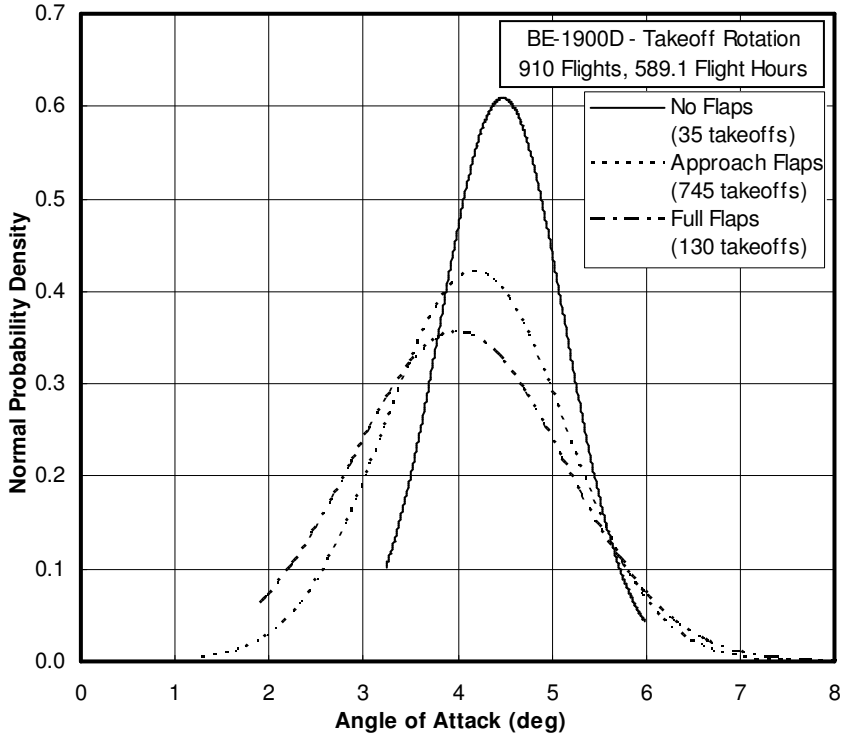

(a) probability density

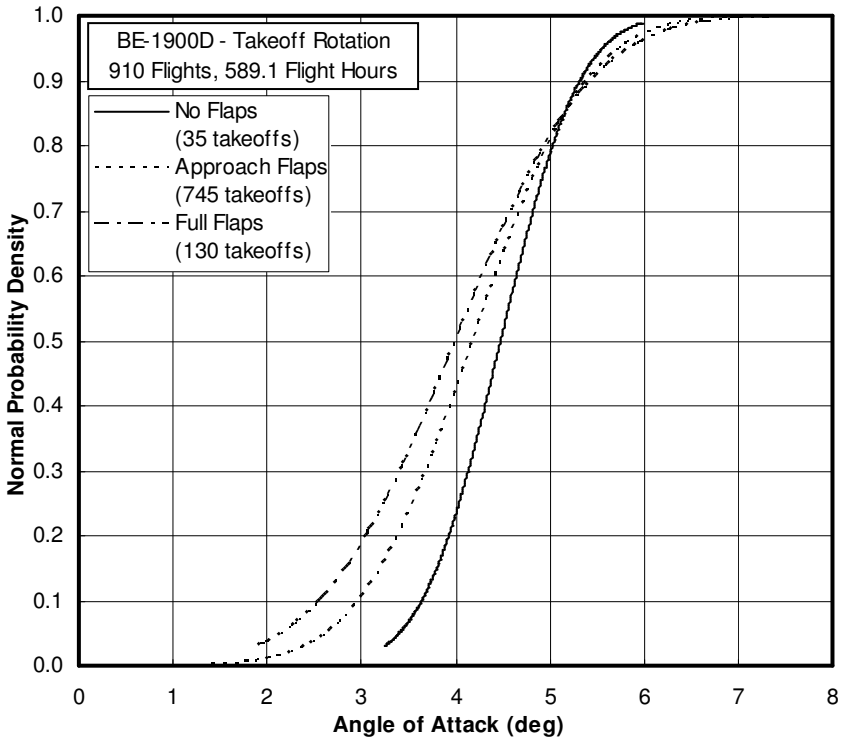

(b) cumulative distribution

Figure 28. Normal distribution of the angle of attack at liftoff

Figure 29 shows a plot of the estimated upwash angle as a function of the true airspeed and altitude above ground level. Curves for altitudes from 0 to 60 feet are shown, as well as a curve for the upwash calculated outside of ground effect. The upwash angle within ground effect is greatly affected by the altitude. On the ground at 110 knots, the upwash angle is almost one degree smaller than the no ground effect case. The difference quickly diminishes, and ground effect becomes negligible when the aircraft reaches an altitude above ground level greater than 50 feet. An aircraft weight of 17,000 lbf was used in the calculation of these angles as information on the actual aircraft weight at takeoff was not known. Maximum takeoff weight for the BE-1900D is roughly equal to 17,000lbf, thus this figure represents the most severe case.

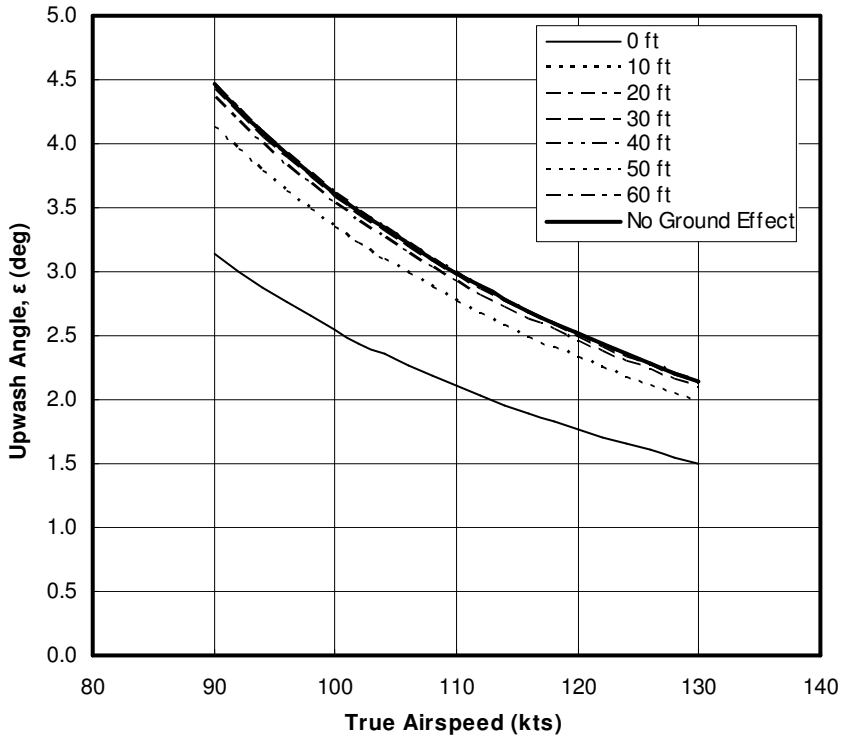

Figure 29. The wing upwash angle while in ground effect plotted as a function of airspeed and altitude above ground level (aircraft weight of 17,000 lbf)

The combination of angle of attack, upwash angle, and engine nacelle tilt angle gives the total inflow angle. Figure 30 shows the distribution of the angle of inflow into the propeller disk at liftoff. The reader is cautioned that the values shown here do not include the nacelle tilt angle. Similar trends to those in Figure 28 are observed in this figure, only now the magnitudes of the angles have increased by about two degrees. The two degree shift represents the estimated upwash angle at liftoff. Again, the result for the no flaps case shown in Figure 30 is unreliable due to the small sample size.

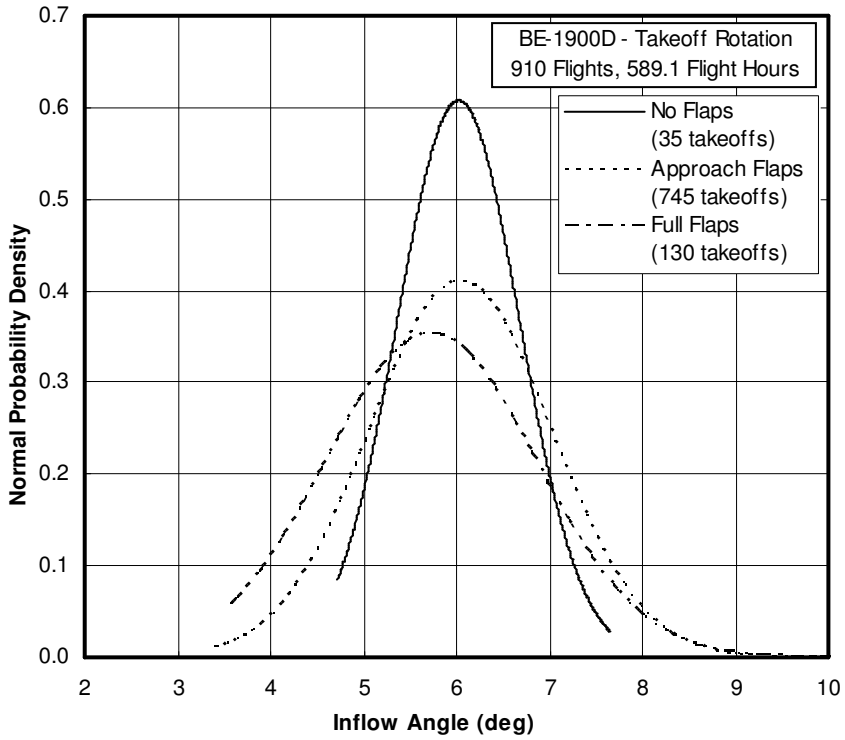

(a) probability density

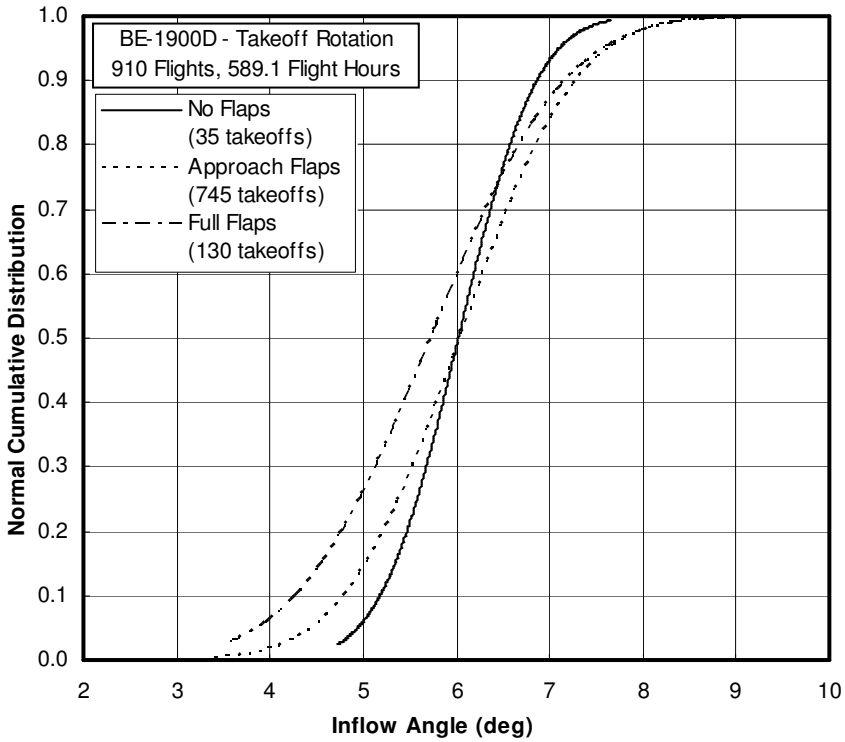

(b) cumulative distribution

Figure 30. Normal distribution of the inflow angle without the nacelle tilt angle at liftoff

The data presented in Figures 28 and 30 shows the angle of attack and inflow angle at liftoff. The reader is reminded that liftoff was defined as the point of maximum angle of attack within ten seconds after rotation. Thus it is likely the aircraft was airborne at this point.

In order to quantify the ground effect upwash reduction, the probability distributions of the liftoff inflow angle with and without ground effect are shown in Figure 31. The data in this figure pertains to cases where takeoff was performed with approach flaps and excludes the nacelle tilt angle. It is clear from this figure that ground effect decreased the upwash angle by about 0.75 degrees, which is significant considering the overall magnitude.

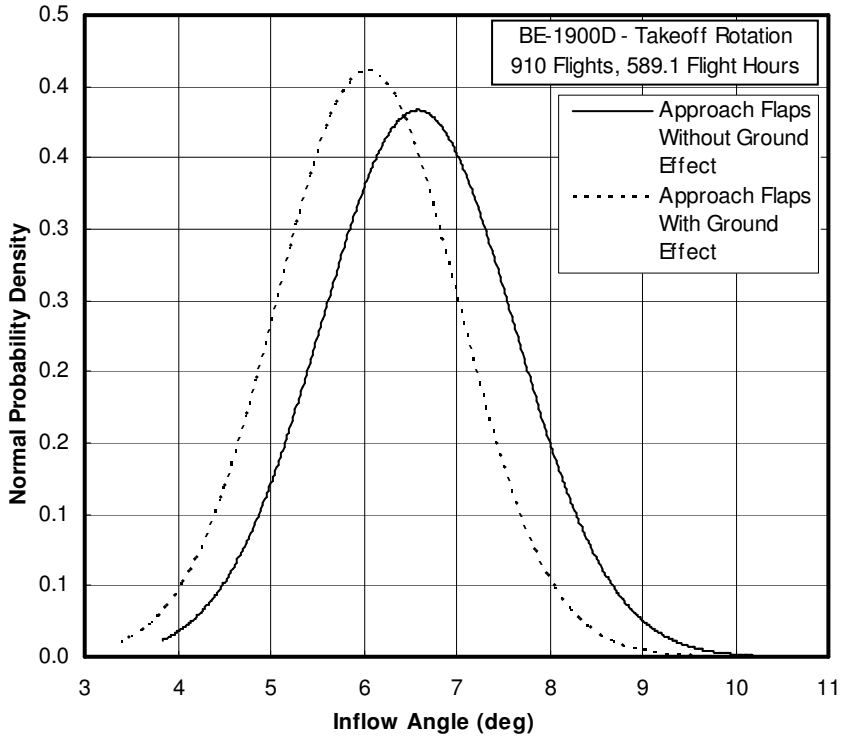

Figure 31. Comparison of normal probability densities of the propeller inflow angle at liftoff with and without ground effect, excluding the nacelle tilt angle

D. FLIGHT OPERATIONS

1. Aerodynamic Data

For each of the five flight phases, the occurrences of angle of attack were extracted and normalized to cumulative occurrences per 1000 hours and per nautical mile. The results are shown in Figure 32. Again, each occurrence corresponded to one second of operation. As expected, the departure phase of flight produced the highest angles of attack. Departure is a transitional phase from takeoff to climb, and consequently, the climbing airspeed is typically higher than that during the departure segment. The lower airspeed results in higher angles of attack during departure compared to climb. The same is true for the airspeeds of cruise compared to climb – cruise airspeeds are significantly higher than climb airspeeds and accordingly, cruise angles of attack are considerably lower.

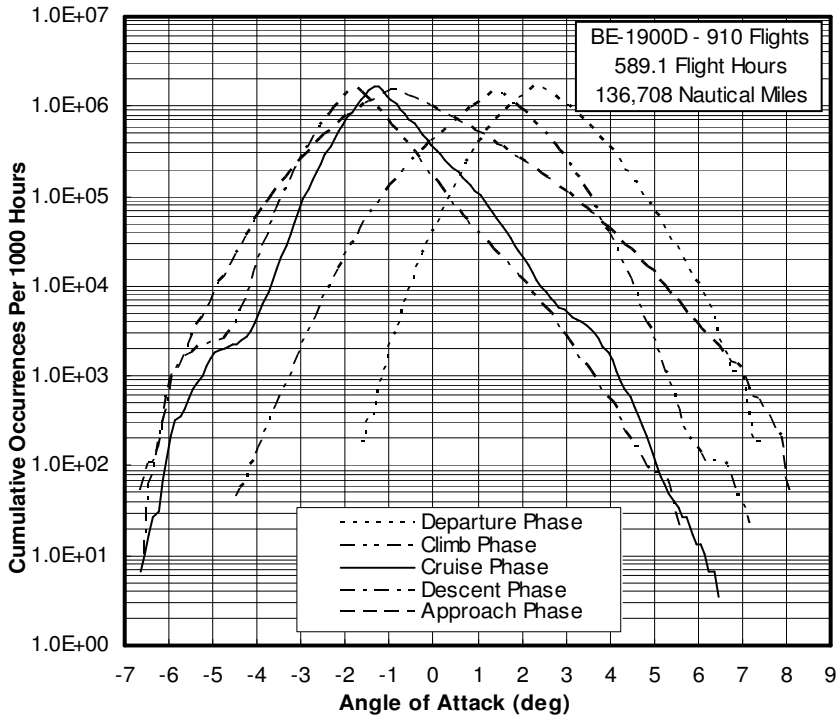

(a) – per 1000 hours

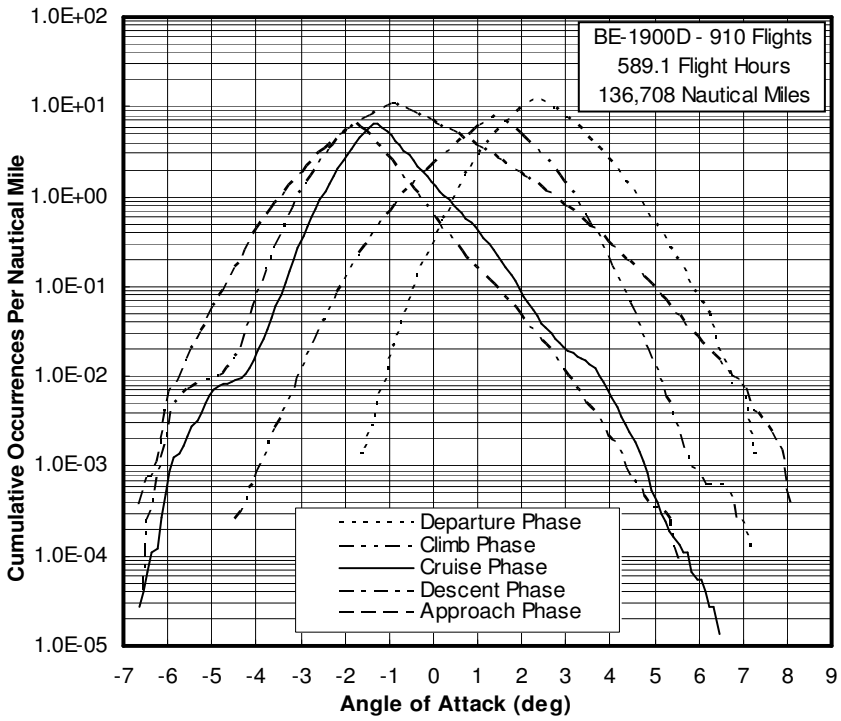

(b) – per nautical mile

Figure 32. Cumulative occurrences of angle of attack during the five flight phases

For descent, the angle of attack plot shows a trend very similar to that of the cruise phase with just a slightly lower mean. Airspeed increases by a small amount in descent from the cruise phases, and thus the small decrease in the attack angles. The mean angle of attack during approach is slightly higher than cruise, but the angles span a wider range. This wide range can be explained by noting that approach serves as a transition phase between descent and landing, and thus a somewhat large airspeed change takes place during this phase. This decrease in airspeed necessitates an increase in angle of attack. A change in flap position from approach to down could also have contributed to this wide range. Approach was identified by a flap deployment from the up position to either approach or down. If approach flaps were initially selected, a change in the angle of attack might occur upon the deployment of full flaps. Flaring

before landing also results in a large increase in the angle of attack, and accordingly, added to the wide range of angles. Aircraft weight also influences the angle of attack, but since takeoff weight was not a known parameter, the data could not be categorized according to this parameter.

Tables 10(a) through (e) present data similar to that in Figure 32. These tables show the angle of attack and coincident dynamic pressure data, presented as percentages of total occurrence. The airspeed (dynamic pressure) relationships between the flight phases discussed above are illustrated in these tables. Departure airspeed is lower than during climb, resulting in higher angles of attack. The same is true for climb compared to cruise. The descent airspeed is slightly higher than cruise, which resulted in slightly lower angles of attack. In Table 10(e) (approach phase), the transitional nature of this phase is clearly illustrated. The airspeeds during approach are slower than during climb, cruise, and descent, and also span a wider range than departure. The airplanes generally cruised within a dynamic pressure range of about 150 to 175 psf, descended at a slightly higher 175 to 200 psf range, and climbed at a low 75 to 100 psf range. Note that the angle of attack range for each flight phase table is unique.

The reader is reminded again that since data was collected at 1 Hz, each occurrence of angle of attack corresponds to one second of flight operation. However, a comparison of the total occurrences given in Table 10 with the information in Figure 15 shows a discrepancy – the values given in Table 10 are all less than what one would obtain from Figure 15. This is a result of the angle of attack not being calculated when the aircraft banked more than five degrees. As a reminder, the method of determining the angle of attack was valid only for small bank angles.

Table 10. Percentage of occurrence of angle of attack and the coincident dynamic pressure for each flight phase

(a) – Departure (17,528 Total Occurrences)

Departure Phase	Dynamic Pressure, q (lb/ft²)										
	0-25	25-50	50-75	75-100	100-125	125-150	150-175	175-200	200-225	225-250	Total
-2.5 to -2	0	0	0	0	0	0	0	0	0	0	0
-2 to -1.5	0	0	0	0.0057	0	0	0	0	0	0	0.0057
-1.5 to -1	0	0	0.0171	0.0171	0	0	0	0	0	0	0.0342
-1 to -0.5	0	0.0399	0.1198	0.0742	0	0	0	0	0	0	0.23
-0.5 to 0	0	0.1198	0.4906	0.1883	0	0	0	0	0	0	0.80
0 to 0.5	0	0.3994	1.4206	0.7588	0	0	0	0	0	0	2.58
0.5 tot 1	0	1.1239	4.2161	1.489	0	0	0	0	0	0	6.83
1 to 1.5	0	1.3864	8.3295	1.4605	0	0	0	0	0	0	11.18
1.5 to 2	0	1.6146	12.785	1.3236	0	0	0	0	0	0	15.72
2 to 2.5	0	1.9968	14.217	0.9471	0	0	0	0	0	0	17.16
2.5 to 3	0	2.4703	12.454	0.3309	0	0	0	0	0	0	15.26
3 to 3.5	0	2.2079	9.8699	0.0856	0	0	0	0	0	0	12.16
3.5 to 4	0	2.1965	6.1958	0.0171	0	0	0	0	0	0	8.41
4 to 4.5	0	1.9055	3.2805	0	0	0	0	0	0	0	5.19
4.5 to 5	0	1.084	1.4662	0.0057	0	0	0	0	0	0	2.56
5 to 5.5	0	0.5306	0.6219	0	0	0	0	0	0	0	1.15
5.5 to 6	0	0.2853	0.1769	0	0	0	0	0	0	0	0.46
6 to 6.5	0	0.1369	0.0685	0	0	0	0	0	0	0	0.21
6.5 to 7	0	0.0342	0.0114	0	0	0	0	0	0	0	0.0456
7 to 7.5	0	0.0114	0.0057	0	0	0	0	0	0	0	0.0171
7.5 to 8	0	0.0057	0	0	0	0	0	0	0	0	0.0057
8 to 8.5	0	0	0	0	0	0	0	0	0	0	0
Total	0	17.55	75.75	6.70	0	0	0	0	0	0	100

(b) – Climb (249,543 Total Occurrences)

Climb Phase	Dynamic Pressure, q (lb/ft²)										
	0-25	25-50	50-75	75-100	100-125	125-150	150-175	175-200	200-225	225-250	Total
-5 to -4.5	0	0	0	0	0	0	0	0	0	0	0
-4.5 to -4	0	0	0	0	0	0	0.0012	0.0028	0	0	0.004
-4 to -3.5	0	0	0	0.0012	0.0012	0.0068	0.0012	0.0024	0	0	0.013
-3.5 to -3	0	0	0	0.0016	0.0152	0.0232	0.0028	0.0008	0	0	0.044
-3 to -2.5	0	0	0.0004	0.004	0.0369	0.0685	0.0421	0.006	0	0	0.16
-2.5 to -2	0	0	0.0012	0.0168	0.1238	0.2144	0.0874	0.0112	0.0028	0	0.46
-2 to -1.5	0	0	0.002	0.0561	0.3599	0.561	0.1719	0.0108	0	0	1.16
-1.5 to -1	0	0	0.004	0.2144	0.8528	0.775	0.2593	0.0353	0	0	2.14
-1 to -0.5	0	0	0.018	0.7462	1.6442	1.191	0.4284	0.0457	0	0	4.07
-0.5 to 0	0	0	0.0641	1.7656	2.5286	1.31	0.3482	0.0337	0.0012	0	6.05
0 to 0.5	0	0	0.2096	4.1183	3.1578	0.9726	0.2661	0.0272	0	0	8.75
0.5 tot 1	0	0	0.5358	8.7957	3.2455	0.5767	0.1362	0.0192	0	0	13.31
1 to 1.5	0	0	0.9582	13.233	2.4918	0.4079	0.0721	0.0028	0	0	17.17
1.5 to 2	0	0	1.4438	13.33	1.7083	0.1675	0.0345	0.0008	0	0	16.68
2 to 2.5	0	0	1.954	10.336	0.8271	0.0701	0.008	0	0	0	13.19
2.5 to 3	0	0.0012	2.3339	6.1208	0.2977	0.022	0.0048	0	0	0	8.78
3 to 3.5	0	0.0004	1.8309	2.7983	0.0886	0.004	0	0	0	0	4.72
3.5 to 4	0	0.002	1.0231	1.1697	0.0144	0.0004	0	0	0	0	2.21
4 to 4.5	0	0.0004	0.4372	0.3438	0.0016	0	0	0	0	0	0.78
4.5 to 5	0	0	0.1619	0.0613	0	0	0	0	0	0	0.22
5 to 5.5	0	0	0.0485	0.0084	0	0	0	0	0	0	0.06
5.5 to 6	0	0	0.0084	0.002	0	0	0	0	0	0	0.010
6 to 6.5	0	0	0.0008	0	0	0	0	0	0	0	0.001
6.5 to 7	0	0	0.002	0	0.0004	0.0004	0	0	0	0	0.003
7 to 7.5	0	0	0.0012	0	0	0	0	0	0	0	0.001
7.5 to 8	0	0	0	0	0	0	0	0	0	0	0
Total	0	0.004	11.04	63.12	17.40	6.37	1.86	0.20	0.004	0	100

Angle of Attack, α (deg)

(c) – Cruise (964,870 Total Occurrences)

Cruise Phase		Dynamic Pressure, q (lb/ft²)										
		0-25	25-50	50-75	75-100	100-125	125-150	150-175	175-200	200-225	225-250	Total
Angle of Attack, α (deg)	-6.5 to -6	0	0	0	0.0006	0	0	0.0028	0	0	0	0.003
	-6 to -5.5	0	0	0	0.0003	0	0.0019	0.0107	0	0	0	0.013
	-5.5 to -5	0	0	0	0.0005	0.0001	0.0131	0.0179	0	0	0	0.032
	-5 to -4.5	0	0	0.0002	0.0006	0.0006	0.0055	0.0103	0.0012	0	0	0.018
	-4.5 to -4	0	0	0.0005	0.003	0.0015	0.0048	0.0197	0.0206	0	0	0.050
	-4 to -3.5	0	0	0.0001	0.0061	0.0038	0.038	0.1969	0.1023	0.0003	0	0.35
	-3.5 to -3	0	0	0.0011	0.0175	0.0137	0.1233	1.1528	0.3385	0.0027	0	1.65
	-3 to -2.5	0	0	0.0027	0.0302	0.0447	0.2952	3.4163	1.1608	0.0047	0	4.95
	-2.5 to -2	0	0	0.0035	0.0465	0.1276	1.2459	7.9789	2.5971	0.0066	0	12.01
	-2 to -1.5	0	0	0.0055	0.0511	0.2643	2.9094	14.078	3.951	0.0231	0	21.28
	-1.5 to -1	0	0	0.0081	0.0738	0.5931	5.0084	14.088	3.6133	0.0257	0	23.41
	-1 to -0.5	0	0	0.0086	0.1203	0.984	5.5025	8.6463	1.4854	0.0087	0	16.76
	-0.5 to 0	0	0	0.0107	0.2144	1.4969	3.3121	3.9631	0.4441	0.0044	0	9.45
	0 to 0.5	0	0.0001	0.0106	0.3194	1.1285	1.4739	1.3835	0.1078	0.0002	0	4.42
	0.5 tot 1	0	0.0005	0.0141	0.4379	0.7133	0.6841	0.6373	0.0339	0	0	2.52
	1 to 1.5	0	0.0005	0.0177	0.5775	0.3902	0.4152	0.233	0.0042	0	0	1.64
	1.5 to 2	0	0.0016	0.0324	0.4404	0.2005	0.116	0.0483	0.0007	0	0	0.84
	2 to 2.5	0	0.002	0.041	0.2033	0.0665	0.0245	0.0091	0	0	0	0.35
	2.5 to 3	0	0.0002	0.0298	0.0636	0.0129	0.0048	0.0015	0	0	0	0.11
	3 to 3.5	0	0	0.0256	0.0188	0.0017	0.0022	0	0	0	0	0.048
	3.5 to 4	0	0	0.0519	0.0047	0.0002	0.0001	0	0.0001	0	0	0.057
	4 to 4.5	0	0	0.0297	0.0013	0.0001	0	0	0.0001	0	0	0.031
	4.5 to 5	0	0	0.0111	0	0	0	0	0	0	0	0.011
	5 to 5.5	0	0	0.0021	0	0	0	0	0	0	0	0.002
	Total	0	0.005	0.31	2.63	6.04	21.18	55.89	13.86	0.076	0	100

(d) – Descent (294,140 Total Occurrences)

Descent Phase		Dynamic Pressure, q (lb/ft²)										
		0-25	25-50	50-75	75-100	100-125	125-150	150-175	175-200	200-225	225-250	Total
Angle of Attack, α (deg)	-6.5 to -6	0	0	0	0	0	0	0	0.0139	0	0	0.014
	-6 to -5.5	0	0	0	0	0.0007	0	0.0007	0.0401	0	0	0.041
	-5.5 to -5	0	0	0	0	0.0014	0.001	0.0037	0.0122	0	0	0.018
	-5 to -4.5	0	0	0	0.0017	0.0041	0.0037	0.0095	0.015	0.001	0	0.035
	-4.5 to -4	0	0	0	0.0092	0.0112	0.0173	0.0986	0.2128	0.0184	0	0.37
	-4 to -3.5	0	0	0.0003	0.0214	0.0306	0.1217	0.4447	1.1478	0.0697	0	1.84
	-3.5 to -3	0	0	0.0034	0.0374	0.1044	0.2628	1.3446	3.3358	0.4008	0	5.49
	-3 to -2.5	0	0	0.0133	0.0483	0.2166	0.7238	2.7949	7.3652	0.6803	0	11.84
	-2.5 to -2	0	0	0.0235	0.0972	0.4783	1.4901	5.1333	11.558	0.9846	0	19.77
	-2 to -1.5	0	0	0.036	0.1326	0.7809	2.32	7.0596	11.648	0.9924	0	22.97
	-1.5 to -1	0	0.0003	0.0619	0.1516	1.145	2.7382	5.306	7.6729	0.5929	0	17.67
	-1 to -0.5	0	0.0003	0.0949	0.2047	1.6873	2.1877	2.6161	3.0999	0.2822	0	10.17
	-0.5 to 0	0	0	0.1363	0.2856	1.3579	1.1138	1.0716	1.1107	0.083	0	5.16
	0 to 0.5	0	0.0014	0.136	0.375	0.7207	0.4318	0.3781	0.3223	0.0337	0	2.40
	0.5 tot 1	0	0.0024	0.1234	0.2713	0.3301	0.154	0.0881	0.0598	0.0065	0	1.04
	1 to 1.5	0	0.0024	0.0901	0.2451	0.1336	0.0313	0.0116	0.0031	0.0014	0	0.52
	1.5 to 2	0	0.0007	0.0615	0.1278	0.1176	0.0095	0.0024	0.0003	0.0014	0	0.32
	2 to 2.5	0	0	0.0394	0.0768	0.0513	0.0007	0	0	0	0	0.17
	2.5 to 3	0	0	0.0405	0.0425	0.0167	0	0	0	0	0	0.10
	3 to 3.5	0	0	0.0204	0.019	0.0037	0	0	0	0	0	0.043
	3.5 to 4	0	0	0.0105	0.0078	0.001	0	0.0003	0.0003	0	0	0.020
	4 to 4.5	0	0	0.0102	0.0003	0.0003	0	0	0	0	0	0.011
	4.5 to 5	0	0	0.0024	0	0	0	0	0	0	0	0.0024
	5 to 5.5	0	0	0.002	0	0	0	0	0	0	0	0.002
	Total	0	0.007	0.91	2.16	7.19	11.61	26.36	47.62	4.15	0	100

(e) – Approach (113,418 Total Occurrences)

Approach Phase		Dynamic Pressure, q (lb/ft²)										
		0-25	25-50	50-75	75-100	100-125	125-150	150-175	175-200	200-225	225-250	Total
Angle of Attack, α (deg)	-6 to -5.5	0	0.0018	0.0185	0.0159	0.0185	0	0	0	0	0	0.055
	-5.5 to -5	0	0.0026	0.0538	0.0555	0.0432	0	0	0	0	0	0.16
	-5 to -4.5	0	0.0035	0.1772	0.1384	0.0899	0	0	0	0	0	0.41
	-4.5 to -4	0.0009	0.0115	0.4259	0.4444	0.2654	0	0	0	0	0	1.15
	-4 to -3.5	0	0.0335	0.932	0.9769	0.3333	0	0	0	0	0	2.28
	-3.5 to -3	0.0106	0.0908	1.6549	1.6347	0.432	0	0	0	0	0	3.82
	-3 to -2.5	0.0317	0.2777	2.8435	2.7826	0.6533	0	0	0	0	0	6.59
	-2.5 to -2	0.0432	0.5281	4.0302	4.0152	0.6807	0	0	0	0	0	9.30
	-2 to -1.5	0.0547	0.8447	5.6217	4.3468	0.5361	0	0	0	0	0	11.40
	-1.5 to -1	0.0529	1.3366	6.5633	3.8742	0.3024	0	0	0	0	0	12.13
	-1 to -0.5	0.0732	1.5782	7.1699	2.6248	0.1525	0.0035	0	0	0	0	11.60
	-0.5 to 0	0.0414	1.7369	6.5298	1.4354	0.0829	0.0026	0	0	0	0	9.83
	0 to 0.5	0.0476	1.617	5.5185	0.8164	0.045	0	0	0	0	0	8.04
	0.5 tot 1	0.03	1.5826	4.3917	0.4038	0.0185	0.0009	0	0	0	0	6.43
	1 to 1.5	0.0247	1.6382	3.19	0.2389	0.0097	0	0	0	0	0	5.10
	1.5 to 2	0.015	1.4724	2.027	0.1146	0.0009	0	0	0	0	0	3.63
	2 to 2.5	0.0115	1.4416	1.1638	0.0441	0	0	0	0	0	0	2.66
	2.5 to 3	0.0097	1.2353	0.6145	0.0388	0	0	0	0	0	0	1.90
	3 to 3.5	0.0053	0.9857	0.276	0.0265	0	0	0	0	0	0	1.29
	3.5 to 4	0.0053	0.7406	0.1437	0.0044	0	0	0	0	0	0	0.89
	4 to 4.5	0.0018	0.5176	0.0397	0.0009	0	0	0	0	0	0	0.56
	4.5 to 5	0.0035	0.3342	0.0141	0	0	0	0	0	0	0	0.35
	5 to 5.5	0.0009	0.201	0.0035	0	0	0	0	0	0	0	0.21
	5.5 to 6	0	0.1084	0.0009	0	0	0	0	0	0	0	0.11
	6 to 6.5	0	0.0467	0	0	0	0	0	0	0	0	0.047
	6.5 to 7	0	0.0256	0	0	0	0	0	0	0	0	0.026
	7 to 7.5	0	0.0229	0	0	0	0	0	0	0	0	0.023
	7.5 to 8	0	0.0097	0.0018	0	0	0	0	0	0	0	0.011
	Total	0.46	18.43	53.41	24.03	3.66	0.007	0	0	0	0	100

In order to extract the total inflow angle experienced during each segment of flight from Table 10, the upwash angle was needed. Figure 33 presents a plot of the calculated upwash angle as a function of the dynamic pressure for various aircraft weights. Departure dynamic pressures of between 25 to 50 psf produced the highest upwash angles – between two and four degrees. This angle decreased quickly and was less than one and a half degree at climb dynamic pressures and about a half degree during cruise. The effect of aircraft weight was much more pronounced at low dynamic pressures. Using information from Figure 33 and Table 10(a), one can see that departure produced the largest inflow angles. Coupled with a high takeoff weight and high power settings, the propeller blades would experience a large inflow angle, and

consequently, large 1P loads during this phase. Figure 33 does not include ground effect and should not be used for extracting the upwash angle at takeoff rotation.

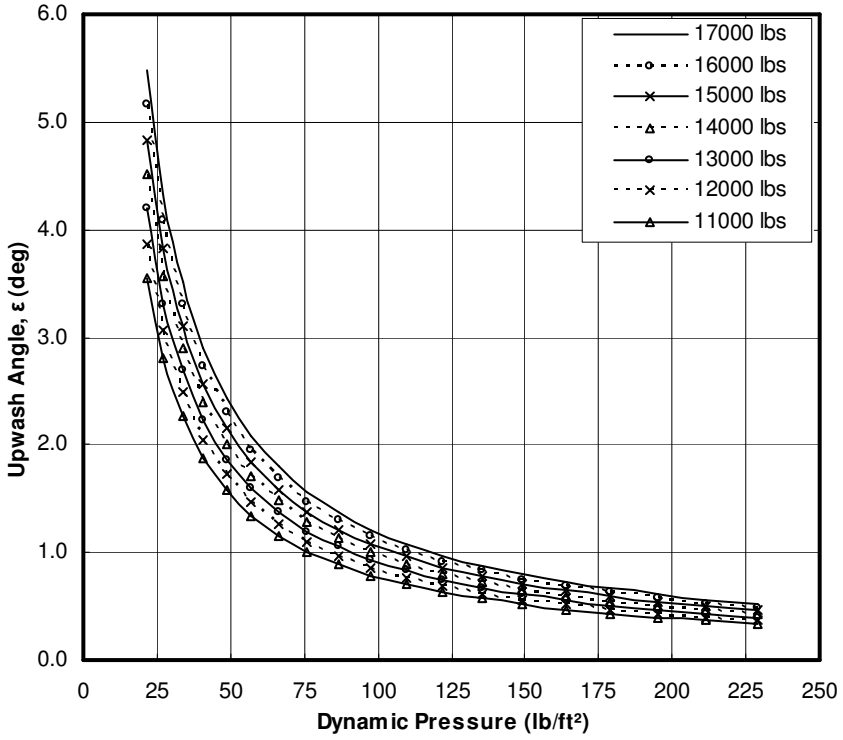

Figure 33. Plot of the upwash angle as a function of dynamic pressure for various aircraft weights

2. In-Flight Engine and Propeller Usage

A correlation of the engine torque and propeller shaft speed, as seen in Table 11, shows how the engines and propellers were used in flight. This table shows the propellers spent the majority of flight time at speeds of 1450 to 1500 RPM and the engines at torque levels between 3000 and 3600 ft-lbf. A typical cruise power setting, as observed in the data files, was a propeller shaft speed of just below 1500 RPM and a torque that varied between 3000 and 3600 ft-lbf, depending on the pressure altitude. The shaft speed during climb was just below 1600 RPM, and thus the smaller peak in percentages for the range between 1550 and 1600 RPM. High torque applied to low shaft speeds was of interest, as well as the frequency of its occurrence. As can be seen in

Table 11, this did not happen often. A torque of more than 3400 ft-lbf was very rarely applied at shaft speeds less than 1450 RPM. An interesting result was the small percentage of shaft speed below 1100 RPM, since the shaft speed was not expected to go that low during flight. However, this is likely due to the method used for identifying a flight by airspeed alone. During a landing, the aircraft touches down at airspeeds greater than 84 knots with the power set to idle, and thus the propeller shaft speed might decrease to these low values.

Table 12 presents data very similar to that in Table 11, but rather correlates the thrust with the shaft speed. Thrust was extracted from the propeller performance maps provided by Hartzell Propeller Inc. The thrust could not be obtained for all flight conditions. In some situations, the power coefficient, the advance ratio, or the propeller tip Mach number was outside the range of the performance maps. This is the reason for the disparity in the percentage of occurrence of the shaft speed between Table 11 and 12. However, Table 12 still shows the same trend in the percentage of operation at different shaft speeds as Table 11 does.

During the majority of the total flight time, thrust was in the 800 to 1200 lbf range. A small percentage of operation between 0 and 200 lbf of thrust is also shown. This likely came from the approach phase, or maybe during a steep descent. Similar to the torque data in Table 11, and unlike the shaft speed data in these two tables, a distinction between the flight phases cannot be made from the thrust percentages.

Table 11. Correlation of engine torque and propeller shaft speed as a percentage of flight time

BE-1900D 910 Flights		RPM/100																	
		< 10	10-10.5	10.5-11	11-11.5	11.5-12	12-12.5	12.5-13	13-13.5	13.5-14	14-14.5	14.5-15	15-15.5	15.5-16	16-16.5	16.5-17	17-17.5	17.5-18	Total
Torque (ft-lbf/100)	0-2	0.0001	7E-05	0.0004	0.0015	0.0057	0.0184	0.0358	0.0524	0.0573	0.0692	0.2216	0.0729	0.1229	0.0249	0.0004	0.0052	0	0.69
	2-4	0.0009	0.0008	0.0012	0.0027	0.0047	0.0069	0.0085	0.0088	0.0087	0.0164	0.2185	0.0496	0.1685	0.0411	7E-05	0.0022	0	0.54
	4-6	0.0012	0.0004	0.0005	0.0005	0.0004	0.0005	0.0007	0.001	0.0023	0.0234	0.3868	0.0702	0.2963	0.0623	2E-05	7E-05	2E-05	0.85
	6-8	0.0004	0.0002	0.0002	0.0002	0.0001	0.0002	0.0002	0.0006	0.0011	0.0199	0.5046	0.1067	0.6758	0.1552	5E-05	0.0001	0	1.47
	8-10	0.0006	0.0001	0.0002	0.0001	0.0002	0.0003	9E-05	0.0003	0.0008	0.0356	0.8329	0.2178	1.1121	0.2295	0.0002	0.0004	0	2.43
	10-12	0.0004	0.0002	5E-05	9E-05	5E-05	9E-05	7E-05	0.0001	0.0009	0.0427	0.9293	0.1673	0.6284	0.1365	0.0001	0.0002	0	1.91
	12-14	0.0002	7E-05	2E-05	7E-05	5E-05	5E-05	2E-05	2E-05	0.0004	0.0833	1.0088	0.1962	0.224	0.0477	2E-05	0	0	1.56
	14-16	2E-05	0	7E-05	0	2E-05	0.0001	0.0006	0.0009	0.0013	0.0677	1.3009	0.2476	0.1228	0.0371	0.0005	0.0007	0.0041	1.78
	16-18	0	2E-05	0.0002	0.001	0.0027	0.0051	0.0077	0.0098	0.0094	0.11	1.6296	0.2456	0.0808	0.0349	0.0005	0.0054	0.0085	2.15
	18-20	0.0002	0.0003	0.0004	0.0002	0.0002	0.0002	0.0002	0.0003	0.0033	0.087	1.5217	0.2623	0.0752	0.0547	0.0004	0.0154	0.0332	2.06
	20-22	0.0002	7E-05	2E-05	5E-05	5E-05	0	0	0	0.003	0.0875	1.4029	0.2626	0.0816	0.0543	0.0007	0.0155	0.031	1.94
	22-24	5E-05	5E-05	2E-05	5E-05	5E-05	0	2E-05	2E-05	0.0012	0.1189	1.7906	0.3775	0.2218	0.1133	0.0001	0.0141	0.0224	2.66
	24-26	5E-05	5E-05	5E-05	0	5E-05	0	0	0	0.001	0.1393	2.9277	0.4757	0.2566	0.1922	0.0004	0.0134	0.0203	4.03
	26-28	2E-05	0	0	2E-05	2E-05	0	0	0	0.0006	0.1878	3.096	0.4417	0.2808	0.3384	0.0022	0.0114	0.019	4.38
	28-30	0	0	0	0	0	0	0	2E-05	0.004	0.4177	6.6936	0.807	0.98	0.9075	0.0084	0.0247	0.0137	9.86
	30-32	0	0	0	0	0	0	0	0	0.0065	0.5995	9.7879	1.3505	2.0891	1.8896	0.0264	0.1119	0.0188	15.88
	32-34	0	0	0	0	0	0	0	0	0.013	0.7518	10.823	1.4321	3.1884	2.3862	0.0515	0.2729	0.0324	18.95
	34-36	0	0	0	0	0	0	0	0	0.0245	1.1538	13.544	2.5905	2.8466	1.7475	0.06	0.4122	0.0557	22.43
	36-37.5	0	0	0	0	0	0	0	0	0.0081	0.244	2.0707	0.8893	0.5214	0.2042	0.0305	0.2395	0.0266	4.23
	> 37.5	0	0	0	0	0	0	0	0	9E-05	0.0057	0.0346	0.0255	0.0279	0.0202	0.0102	0.0797	0.0048	0.209
	Total	0.0044	0.0024	0.0033	0.007	0.014	0.032	0.054	0.074	0.15	4.26	60.73	10.29	14.00	8.68	0.19	1.23	0.29	100

Table 12. Correlation of thrust and propeller shaft speed as a percentage of flight time

BE-1900D 910 Flights		RPM/100																	
		< 10	10-10.5	10.5-11	11-11.5	11.5-12	12-12.5	12.5-13	13-13.5	13.5-14	14-14.5	14.5-15	15-15.5	15.5-16	16-16.5	16.5-17	17-17.5	17.5-18	Total
Thrust (lbf/100)	0-2	0.0074	0.0035	0.0045	0.0087	0.0179	0.0367	0.06	0.08	0.0958	0.5918	3.7945	0.4522	0.9477	0.182	0.0007	0.0074	2E-05	6.29
	2-4	0	0	0	0	0	0	0	0	0.0004	0.0288	1.1156	0.3022	0.7372	0.1493	0.0001	9E-05	0	2.33
	4-6	0	0	0	0	0	0	0	2E-05	0.0015	0.1389	2.2061	0.4972	1.4626	0.2888	0.0002	0.0004	0	4.60
	6-8	0	0	0	0	0	0	0	0	0.0031	0.3386	6.2763	1.0377	0.6594	0.1577	0.0007	5E-05	0	8.47
	8-10	0	0	0	0	0	0	0	0	0.0187	1.6607	21.729	2.6403	0.3818	0.2344	0.0001	0.0003	0.0079	26.67
	10-12	0	0	0	0	0	0	0	0	0.0512	1.2891	25.75	4.8295	1.5046	1.4194	0.0015	0.0007	0.0111	34.86
	12-14	0	0	0	0	0	0	0	0	0.0003	0.0214	0.4759	0.1975	2.3075	2.42	0.005	0.0023	0.0218	5.45
	14-16	0	0	0	0	0	0	0	0	0	0.0003	0.0131	0.0796	3.1535	2.2766	0.0099	0.0063	0.0051	5.54
	16-18	0	0	0	0	0	0	0	0	0	0	0.0002	0.0675	2.3182	1.3475	0.0217	0.0232	0.0116	3.79
	18-20	0	0	0	0	0	0	0	0	0	0	7E-05	0.0047	0.3484	0.2393	0.0543	0.152	0.0177	0.82
	20-22	0	0	0	0	0	0	0	0	0	0	2E-05	2E-05	0.0193	0.0214	0.0421	0.353	0.0353	0.47
	22-24	0	0	0	0	0	0	0	0	0	0	0	0	0.0018	0.0007	0.0216	0.2666	0.0312	0.32
	24-26	0	0	0	0	0	0	0	0	0	0	0	0	0.0006	0.0001	0.0158	0.171	0.0174	0.20
	26-28	0	0	0	0	0	0	0	0	0	0	0	0	0.0003	0	0.0112	0.108	0.0106	0.13
	28-30	0	0	0	0	0	0	0	0	0	0	0	0	9E-05	0	0.0027	0.0373	0.0045	0.045
	30-32	0	0	0	0	0	0	0	0	0	0	0	0	0	0	0	0.0014	0.0003	0.0017
	32-34	0	0	0	0	0	0	0	0	0	0	0	0	0	0	0	0.0003	0	0.0003
	> 34	0	0	0	0	0	0	0	0	0	0	0	0	0	0	0	0	0	0
	Total	0.0074	0.0035	0.0045	0.0087	0.0179	0.0367	0.06	0.0801	0.17	4.07	61.36	10.11	13.84	8.74	0.19	1.13	0.17	100

3. Gust Loads

This section presents the results of the derived gust velocity data extracted from normal accelerations. Derived gust velocities were converted into changes in the propeller inflow angle and presented here as the cumulative occurrences per 1000 hours and per nautical mile. The reader is reminded again that each occurrence had a duration of one second. The data was separated by flight phase and divided into various altitude bands indicated on the figures.

Figure 34 shows the cumulative occurrences of the change in inflow angle during the climb phase of flight. Generally, with increasing altitude turbulence decreases. A major cause of turbulence is solar heating of the earth's surface which results in thermals, and consequently, as altitude increases turbulence generally becomes less severe. This is observed in Figure 34 which shows a trend of decreasing occurrences with increasing altitude, as well as decreasing magnitude of the change in inflow angle. The altitude band between 0 and 500 ft did not follow this trend exactly. The reason for this is likely due to the very small amount of time spent within this range, and thus, even though the data was normalized, the results are distorted. It is important to note that the data presented here pertains to gusts only and only if the two-second rule for separation of gusts loads and maneuver loads is applicable.

Figure 34 also shows that the magnitudes of positive changes in the inflow angle were generally greater than negative changes. When a change of a specific angle is considered, a one degree change for example, the positive changes are observed to have occurred more frequently than the negative inflow angle changes.

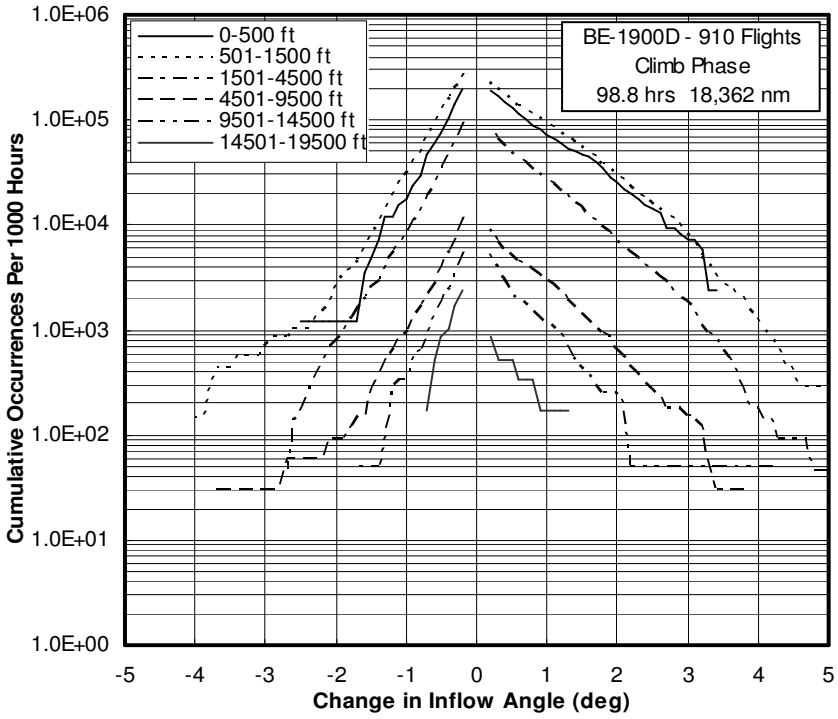

(a) – per 1000 hours

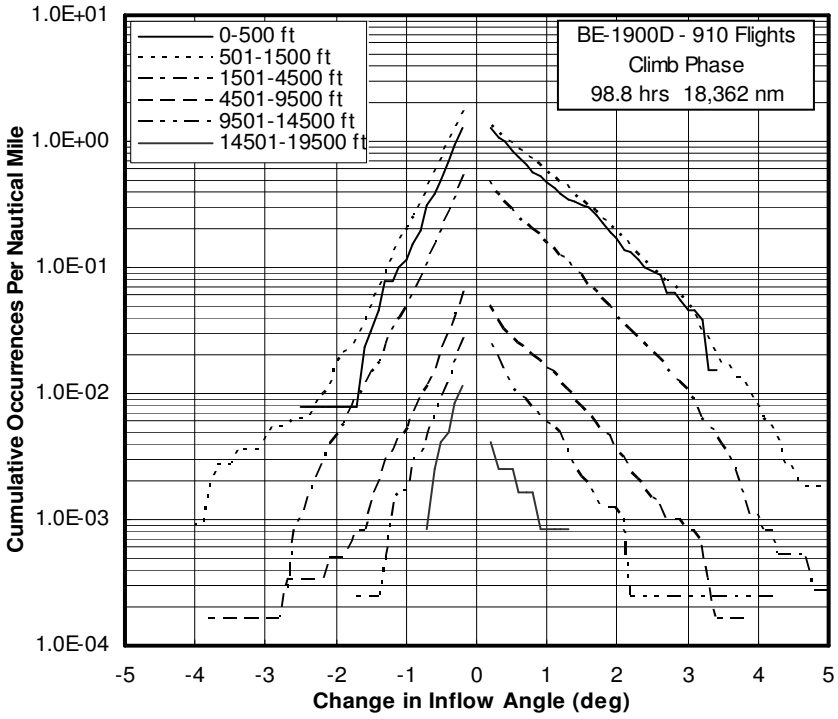

(b) – per nautical mile

Figure 34. Cumulative occurrence of the change in the total inflow angle due to gusts during climb

Figure 35 presents the same data for the cruise phase of flight. Again a similar trend to that in Figure 34 is observed. The 501 to 1500 ft altitude band in this figure also did not follow the exact same pattern as the other altitude bands. This is again due to a very small amount of cruise time spent in this altitude band. The aircraft cruised at this altitude for a short time probably only after descending and before transitioning into the approach phase. Similar to the climb phase, an increase in inflow angle also showed a greater frequency of occurrence than a decrease in the angle. For a specific altitude band, the number of occurrences during cruise was about an order of magnitude less than during the climb phase. This is a direct result of the difference in airspeed between the two phases. For example, a derived gust velocity of 10 feet per second occurring while climbing at 170 knots would cause a change in inflow angle of about 2 degrees. The same turbulence intensity while cruising at 220 knots would result in a change in inflow angle of 1.5 degrees. Thus, when comparing the data for different flight phases, the airspeed of each phase have to be taken into account.

A comparison of the cruise phase to the descent phase, Figure 36, indicates that the frequency of occurrence within similar altitude bands was comparable. This is due to the similar airspeed during these two phases. The traits observed in Figure 36 further showed no significant discrepancies with those observed in the Figures 34 and 35. The aircraft cruised within an altitude band between 19,501 and 24,500 feet, but Figures 34 and 36 do not have that band. The aircraft had to climb and descend within this altitude band, so it was concluded that the aircraft did not experience any significant turbulence while climbing and descending in this range. This conclusion is supported by Figure 35 which shows the aircraft experienced the least turbulence while cruising above 19,500 feet.

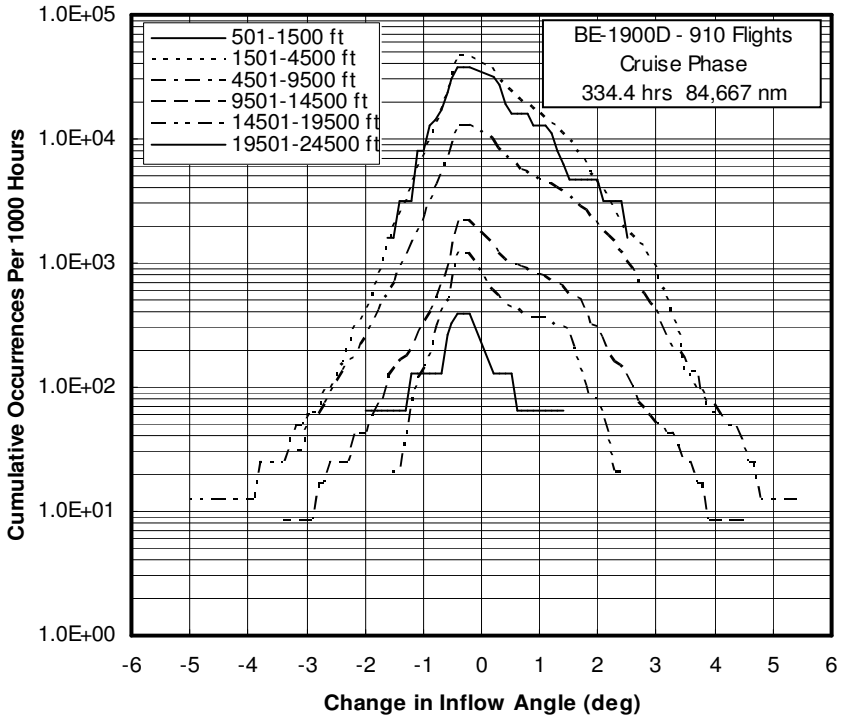

(a) – per 1000 hours

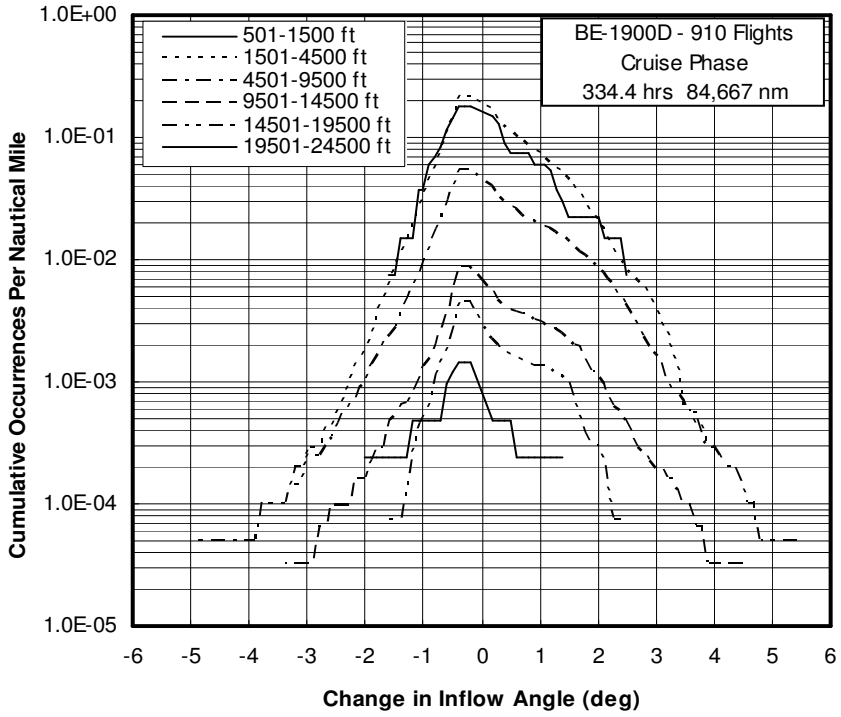

(b) – per nautical mile

Figure 35. Cumulative occurrence of the change in the total inflow angle due to gusts during cruise

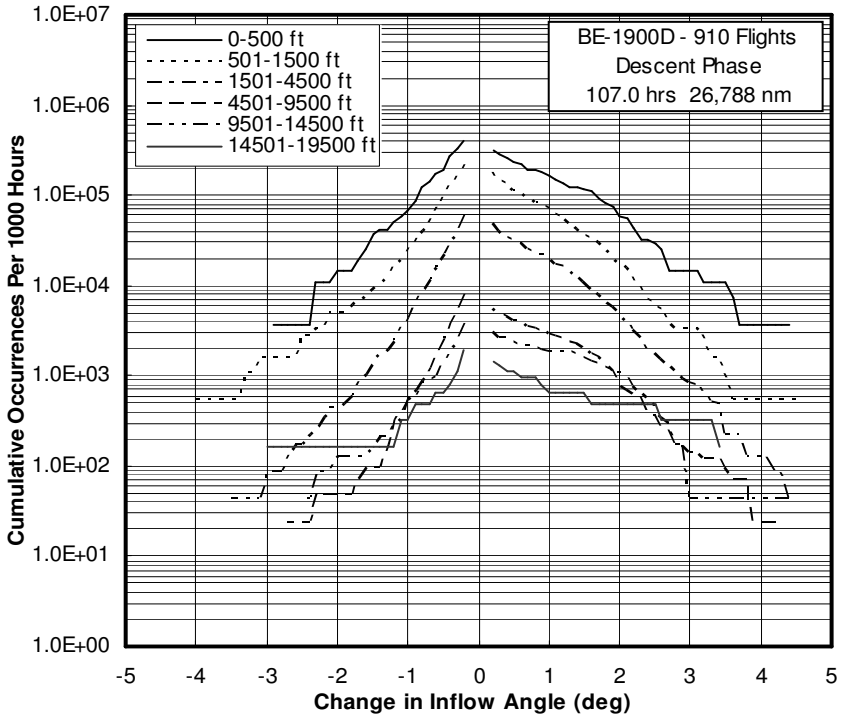

(a) – per 1000 hours

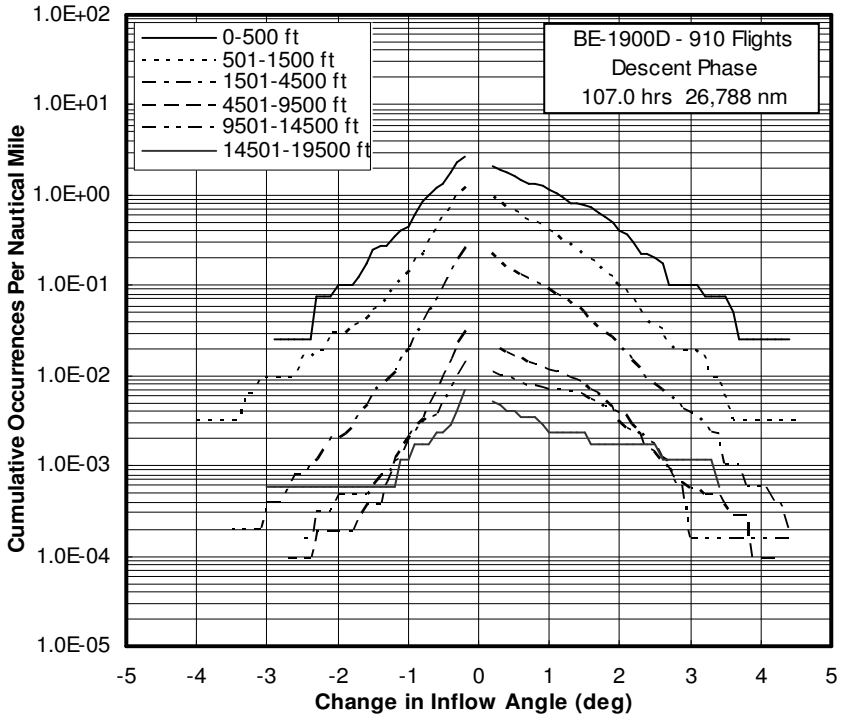

(b) – per nautical mile

Figure 36. Cumulative occurrence of the change in the total inflow angle due to gusts during descent

E. CHAPTER SUMMARY

This chapter presented the results obtained from the processing of 589 hours of flight operations data recorded from a fleet of Beechcraft 1900D aircraft in commuter airline service. Information on the overall aircraft usage was presented to describe the commuter airline flight profile. Ground operations were divided into three categories – general ground operations, reverse propeller, and takeoff rotation. The short duration takeoff rotation phase was given special attention as this was deemed the most severe case in terms of blade loading, as well as operations within prohibited shaft speed ranges. Flight operations were divided into five phases and aerodynamic and turbulence figures pertaining to each phase was presented. The usage of the engines and propellers while in flight were also considered.

IV. CONCLUSIONS

Data obtained from digital flight data recorders were used to assess the actual operational environment of propellers on a fleet of Beech 1900D aircraft in the commuter airline role. Information was presented on the overall aircraft and subsystem usage, ground operations parameters pertaining to the engines and propeller as well as flight operations that included various aerodynamic parameters.

The aircraft were mostly operated on short flights, which averaged about 39 minutes in duration. This flight duration is typical of the commuter airline role. The flap operations figures indicated takeoffs were mostly performed with approach flaps while landings were generally executed with full flaps. Flight with the flaps in an extended position contributed to a very small percentage of the total flight time. Examination of the airspeed at flap retraction indicated the maximum flaps extended airspeeds was rarely exceeded. Each flight was divided into five phases. The majority of a flight was spent in cruise with the approach and departure phases accounting for very small percentages of the total airborne time.

Ground operations were given special attention with regard to the prohibited shaft speed ranges. Operation of the propellers within the lower restricted band for more than 30 seconds accounted for about 10% of the total time on the ground. This is a significant amount of time within a prohibited propeller shaft speed range. The right engine was also shown to have been used more than the left, and this was concluded to be a result of shutdowns of the left engine primarily for loading and unloading without complete system shut down. This was also likely for reduced fuel burn by taxiing with one engine. Transitioning time through the restricted shaft speed ranges showed nothing out of the ordinary.

Reverse propeller usage indicated a more frequent use during ground operations than during the landing rollout. In fact, simultaneous propeller reversals occurred on only 320 of the 910 landings, and landings only accounted for about 38% of the total number of reversals. The data files indicated minor inconsistencies between the start times of the left and right propeller reversals during the landing rollout. This inconsistency is postulated to be the reason for not using reverse thrust during the landing rollout as the resulting yawing moment could cause great discomfort for the passengers. Reverse cycles during ground operations were concluded to be for braking and ground maneuvering.

The short duration takeoff rotation was identified as the most demanding phase of flight in terms of magnitude of the periodic loads exerted on the propeller blades. Rotation airspeed average was around 112 knots, and the torque and shaft speed parameters indicated the engines were generally at full power for takeoff. The flap position showed to have an influence on the angle of attack at liftoff – a greater flap deflection showed a decrease in angle of attack. Due to a small sample size for takeoffs without flaps, the result for this case was deemed unreliable. Angle of attack at liftoff for the most common case (approach flaps) was about 4.2 degrees, and the full flap takeoffs averaged about 4 degrees.

Upwash angle was estimated using an equivalent horseshoe vortex system for a range of dynamic pressures and aircraft weights. This parameter was shown to have significant influence on the inflow angle at the plane of the propeller, especially at low dynamic pressures and high gross weights. The upwash angle at liftoff, which included the ground effect, was estimated to be about 2 degrees. The reduction in the upwash angle due to ground effect was estimated to be about 0.75 degrees. High power settings coupled with high angles of attack and high upwash angles at liftoff were believed to lead to high vibratory loads on the propeller disks.

Angle of attack was extracted from the flight parameters and was shown to vary from -6 to +8 degrees, depending on the flight phase. Cumulative occurrences of this parameter were presented per nautical mile and per 1000 hours of operation. Each flight phase had a unique variation of the in flight angle of attack. Departure produced the highest angles and descent the lowest, while approach indicated a wide spread of angles. The mean angles of attack as well as the distribution of the angles experienced during flight were attributed to the airspeed associated with each phase.

Correlations of torque and thrust with the propeller shaft speed were also presented and proved to show no unusual traits. High engine torques applied to low shaft speeds were also considered. Torque levels greater than 3600 ft-lbf were very rarely applied at shaft speeds below 1450 RPM; the typical cruising shaft speed was between 1450 and 1500 RPM.

Gust loads were extracted from the normal accelerations data and converted to the change in propeller inflow angle. This data was also presented as cumulative occurrences per nautical mile and per 1000 hours. A trend of decreasing occurrences and magnitude with increasing altitude was observed. Increased airspeed was also shown to decrease the severity of the inflow angle change.

The above information was presented in statistical formats that could enable the FAA, the propeller manufacturer, and the airline to better understand and control those factors that influence the structural integrity of these components.

REFERENCES

LIST OF REFERENCES

[1] Carrol, T. J. "Wright Brothers' Invention of 1903 Propeller and Genesis of Modern Propeller Theory," *Journal of Aircraft*, Volume 42, Number 1, January-February 2005, pp. 218-223

[2] Mack, P. E. *From Engineering Science to Big Science: The NACA and NASA Collier Trophy Research Project Winners*, Chapter 14, The NASA History Series, 1998

[3] Veldhuis, L. L. M. "Propeller Wing Aerodynamic Interference," Delft University of Technology, PhD Dissertation, 2005

[4] Arnoult, S. "Turboprop Revival," *Air Transport World*, May 2006, pp. 57-58

[5] Bombardier Inc. 2007-2008 Annual Report, pp. 44-77

[6] Finmeccanica, 2007 Annual Report, pp. 44-49

[7] Finmeccanica 2006 Annual Report, pp. 49-53

[8] Tipps, D. O., Skinn, D. A., Rustenberg, J. W. "Statistical Loads Data for BE-1900D Aircraft in Commuter Operations," Department of Transportation Report DOT/FAA/AR-00/11, April 2000

[9] Burden, M., McCarthy, R., Wiggins, B. "Advanced Polymer Composite Propeller Blades," *Aerospace Materials*, MPG Books Ltd, Bodmin, Cornwall, UK, 2001, Chap. 6

[10] McCarthy, R. "Manufacture of Composite Propeller Blades for Commuter Aircraft," SAE Paper 850875, SAE 1985 Transactions, Section 4, Volume 94, 1985, pp. 606-613

[11] Brahney, J. H. "Composite Propellers: Some Pros and Cons," *Aerospace Engineering*, Volume 6, Number 5, May 1986, pp. 12-19

[12] Colclough, W. J. "How Well Do Composite Propellers Weather?" *Aerospace Engineering*, Volume 4, July/August 1984, pp. 47-51

[13] Anon. *Jane's All the World's Aircraft 2004-2005*, Franklin Watts, New York, 2004

[14] FAA Type Certificate Data Sheet Number P-10NE, Revision 17, 4 September 2007

[15] Harlament, W. B., Edinger, R. "Development of an Aircraft Composite Propeller," SAE Paper 790579, Society of Automotive Engineers, Business Aircraft Meeting and Exposition, Wichita, KS, United States, 3-6 Apr. 1979

LIST OF REFERENCES (Continued)

[16] Advisory Circular, AC 20-66A, "Vibration and Fatigue Evaluation of Airplane Propellers," September 2001

[17] FAA Type Certificate Data Sheet Number A24CE, Revision 96, pp. 36-41, 20 November 2007

[18] Advisory Circular, AC 35.37-1A, "Guidance Material for Fatigue Limit Tests and Composite Blade Fatigue Substantiation," September 2001

[19] Dommasch, D. O., *Elements of Propeller and Helicopter Aeroidynamics*, Pitman Publishing Corporation, New York, 1953

[20] Law, A.M., Kelton, W. D., *Simulation Modeling and Analysis*, McGraw Hill Higher Education, 3rd Edition, April 2000, Chap. 6